

Czech Technical University in Prague  
Faculty of Nuclear Sciences and Physical Engineering  
Department of Physics



## **Non-Gaussian Boson Sampling**

by

*Meet Rajkumar Panchal*

A Diploma Thesis submitted to  
the Faculty of Nuclear Sciences and Physical Engineering, Czech Technical  
University in Prague,  
in partial fulfilment of the requirements for the degree of Master.

Master's degree study programme: Quantum Technologies

Prague, May 2024

---

**Supervisor:**

Dr. Craig Hamilton  
Department of Physics  
Faculty of Nuclear Sciences and Physical Engineering  
Czech Technical University in Prague  
Břehová 78/7, Staré Město  
115 19 Prague 1  
Czech Republic

Copyright © 2024 Meet Rajkumar Panchal

## I. Personal and study details

Student's name: **Panchal Meet Rajkumar** Personal ID number: **519846**  
Faculty / Institute: **Faculty of Nuclear Sciences and Physical Engineering**  
Department / Institute: **Department of Physics**  
Study program: **Quantum Technologies**

## II. Master's thesis details

Master's thesis title in English:

**Non-Gaussian Boson Sampling**

Master's thesis title in Czech:

**Vzorkování bosonů z negaussovských stavů**

Guidelines:

Student will study the interference of non-Gaussian bosonic states interfering through linear interferometers.

- 1) Write programs to calculate output statistics
- 2) Analyze and interpret results from programs

Bibliography / sources:

- [1] Aaronson, Arkhipov, Alex (2013). "The computational complexity of linear optics". Theory Comput. 9, 143 (2013).
- [2] Hamilton et al, 2017 "Gaussian Boson Sampling". Phys. Rev. Lett. 119, 170501 (2017).

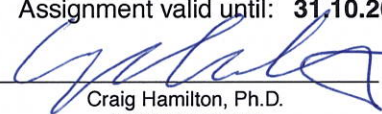
Name and workplace of master's thesis supervisor:


**Craig Hamilton, Ph.D. Department of Physics FNSPE**

Name and workplace of second master's thesis supervisor or consultant:

Date of master's thesis assignment: **31.10.2023** Deadline for master's thesis submission: **10.05.2024**

Assignment valid until: **31.10.2025**

  
Craig Hamilton, Ph.D.  
Supervisor's signature

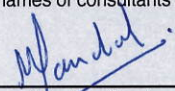
  
Head of department's signature

  
doc. Ing. Václav Čuba, Ph.D.  
Dean's signature

## III. Assignment receipt

The student acknowledges that the master's thesis is an individual work. The student must produce his thesis without the assistance of others, with the exception of provided consultations. Within the master's thesis, the author must state the names of consultants and include a list of references.

13.2.2024  
Date of assignment receipt

  
Student's signature



## PROHLÁŠENÍ

Já, níže podepsaný

*Jméno a příjmení studenta:* Meet Rajkumar Panchal  
*Osobní číslo:* 519846  
*Studijní program:* Quantum Technology (P\_QTNAJ)  
*Studijní obor:* /  
*Specializace:* /

prohlašuji, že jsem diplomovou prací s názvem:

### **Non-Gaussian Boson Sampling**

vypracoval samostatně a uvedl veškeré použité informační zdroje v souladu s Metodickým pokynem o dodržování etických principů při přípravě vysokoškolských závěrečných prací.

Rovněž souhlasím s porovnáním textu mé kvalifikační práce s databází kvalifikačních prací Theses.cz provozovanou Národním registrem vysokoškolských kvalifikačních prací a systémem na odhalování plagiátů.

V Praze dne 10.05.2024

.....  
podpis

---

# Abstrakt

Kvantové technologie jsou již několik desetiletí středem zájmu výzkumu a vykazují slibný pokrok oproti klasickým technologiím. Koncept kvantové nadřazenosti zdůrazňuje kvalitativní výpočetní výhodu kvantových počítačů oproti klasickým. Tato zařízení mohou řešit problémy, které jsou pro klasické počítače prakticky neřešitelné v rozumném časovém horizontu.

Navzdory očekáváním spojeným s vývojem plně funkčních kvantových počítačů se značným počtem qubitů pod koherentní kontrolou je tento milník vzdálen ještě několik let. Prokázání kvantové nadřazenosti však nutně nevyžaduje univerzální kvantový počítač.

Tato práce se zaměřuje konkrétně na problém bosonového vzorkování a je strukturována do tří hlavních oblastí zkoumání. Zaprvé se zabývá kvantovou optikou, aby získala teoretické nástroje nezbytné pro pochopení bosonového vzorkování. Za druhé, zkoumá vývoj protokolů Boson Sampling, aby posoudila jejich výkonnost. Nakonec představuje výsledky výzkumu bosonového vzorkování s negaussovskými stavy.

**Keywords:**

Vzorkování Bosonů, Kvantová Optika, Kvantová Nadřazenost.

---

# Abstract

Quantum technologies have been a focal point of research for decades, showing promising advancements over classical counterparts. The concept of Quantum Supremacy underscores the qualitative computational advantage quantum computers hold over classical ones. These devices can address problems that are practically infeasible for classical computers to solve within reasonable time frames.

Despite the anticipation surrounding the development of fully functional quantum computers with a significant number of qubits under coherent control, this milestone is still a few years away. However, demonstrating quantum supremacy doesn't necessarily require a universal quantum computer.

This thesis centers specifically on the Boson Sampling problem and is structured around three primary areas of investigation. Firstly, it delves into Quantum Optics to acquire the theoretical tools essential for comprehending Boson Sampling. Secondly, it scrutinizes the evolution of Boson Sampling protocols to assess their performance. Lastly, it presents research outcomes on Boson Sampling with Non-Gaussian states.

**Keywords:**

Boson Sampling, Quantum Optics, Quantum Supremacy.

---

# Acknowledgements

First and foremost, I would like to express my heartfelt gratitude to my master's thesis supervisor, Dr. Craig Hamilton, and my mentor, Dr. Antonín Hoskovec, for their unwavering encouragement and insightful guidance during my research journey. Their assistance with numerous challenges and contributions to my professional development have been invaluable. Additionally, I extend my thanks to Dr. Martin Stefanik for generously providing essential computational resources and offering consistent support throughout my master's degree program.

I extend special thanks to the staff of the Department of Physics, Faculty of Nuclear Science and Physical Engineering at the Czech Technical University, whose efforts have cultivated a pleasant and flexible environment conducive to my research. Additionally, I want to express my gratitude to Dr. Václav Potoček for generously sharing crucial insights into Quantum Optics beyond regular class hours, proving to be immensely beneficial for my project. Last but not least, my deepest appreciation goes to my family members for their boundless patience and unwavering care.

---

## Help from AI

In pursuit of refining the language and ensuring grammatical correctness in this diploma thesis, I have availed myself of AI services such as ChatGPT, in compliance with the regulations stipulated by the institute regarding the use of AI assistance. The services utilized in the present work are as follows:

1. Help in fixing Grammatical and spelling mistakes.
2. Rephrasing of sentences for better readability.

However, it's important to note that the content of this thesis is original, and any borrowed parts are meticulously cited in accordance with the rules and guidelines.



---

# Contents

<b>1</b>	<b>Introduction to Quantum Optics</b>	<b>1</b>
1.1	The Photon . . . . .	1
1.2	History . . . . .	1
1.3	Quantum Theory of Light . . . . .	2
1.4	Quantization of Electromagnetic Field . . . . .	2
1.5	States in Quantum Mechanics . . . . .	8
1.5.1	Pure States . . . . .	8
1.5.2	Mixed States . . . . .	8
1.6	Single Mode States . . . . .	9
1.6.1	Fock States . . . . .	9
1.6.2	Coherent States . . . . .	10
1.6.3	Squeezed States . . . . .	11
1.6.4	Thermal States . . . . .	14
1.7	Photon Interference at a Beam Splitter . . . . .	14
<b>2</b>	<b>Boson Sampling</b>	<b>17</b>
2.1	Boson Sampling - The Model . . . . .	17
2.1.1	Experimental Factors - AABS . . . . .	20
2.2	Scattershot Boson Sampling . . . . .	21
2.2.1	Experimental Factors - SBS . . . . .	23
2.3	Gaussian Boson Sampling . . . . .	24
2.3.1	Experimental Factors - GBS . . . . .	28
2.4	Non Gaussian Boson Sampling . . . . .	29
2.4.1	Experimental Factors - NGBS . . . . .	31
<b>3</b>	<b>Our Methodology</b>	<b>32</b>
3.1	Non Gaussian States of Light . . . . .	32
3.2	Simulating Boson Sampling on a Classical Computer . . . . .	32
3.2.1	Two Mode Interference . . . . .	33

3.2.2	Three Mode Interference . . . . .	34
3.2.3	Four Mode Interference . . . . .	36
3.3	Analytical Results . . . . .	37
3.3.1	Two Mode Calculation . . . . .	37
3.3.2	Three Mode Calculation . . . . .	38
3.3.3	Four Mode Calculation . . . . .	40
<b>4</b>	<b>Observation of Photon Bunching</b>	<b>42</b>
4.0.1	Two Modes . . . . .	44
4.0.2	Three Modes . . . . .	45
4.0.3	Four Modes . . . . .	45
4.0.4	Five Modes . . . . .	46
4.0.5	Six Modes . . . . .	47
4.0.6	Diminishing Trend . . . . .	47
4.0.7	Correlation Analysis using Random Interferometers . . . . .	48
<b>5</b>	<b>Conclusions</b>	<b>50</b>
<b>6</b>	<b>Future Direction of Work</b>	<b>51</b>
	<b>Bibliography</b>	<b>52</b>

---

# Introduction to Quantum Optics

## 1.1 The Photon

We refer to the photon as a quanta of the electromagnetic field or describe a light beam as consisting of flowing particles called photons. In the context of Quantum Optics, as outlined in[1], a photon is conveniently expressed for an electromagnetic field confined within a perfectly reflecting cavity. By considering the boundary conditions at the cavity walls, the field excitations are composed of an infinite discrete set of spatial modes. In the quantum description, the evolution of each mode is governed by the equations of the quantum harmonic oscillator. A quantum harmonic oscillator exhibits a discrete energy value spectrum, with eigenvalues being integral multiples of  $n\hbar\omega$ , where  $n$  is the eigenvalue of the number operator. In this framework, a spatial mode associated with a harmonic oscillator in the  $n^{\text{th}}$  excited state contains  $n$  photons with a uniform spatial distribution within the cavity. This perspective provides a more accurate and nuanced understanding within the context of Quantum Optics.

## 1.2 History

In the early 20<sup>th</sup> century, the quantum theory of light began to take form as Max Planck postulated quantized energy levels for a harmonic oscillator. This formulation allowed him to account for the spectral distribution of electromagnetic energy emitted by thermal sources[2][3]. Subsequently, in 1905, Albert Einstein[4] explained the photoelectric effect by considering the particle nature of light—the quanta of electromagnetic fields, later termed photons by Lewis in 1926. Einstein further laid the foundations of light-matter interaction in 1917 through his model of absorption and emission of electromagnetic radiation by an atom[5].

A semiclassical theory is one in which the participating electromagnetic fields are considered classical, while atoms are described using quantum theory. To establish a complete quantum theory, the electromagnetic field itself needed to be quantized, a step formalized

by Dirac in[6]. However, not all phenomena necessitated quantum theory for accurate predictions. Classical theories sufficed for interpreting properties observed in interference experiments like Young's Double Slit and the Hanbury Brown and Twiss Interferometer.

The full quantum theory of light emerged after the invention of the laser by Maiman in 1960[7]. The high coherence of the laser's emitted beam enabled experiments that could only be interpreted by the complete quantum theory of light. The field of Quantum Optics essentially took shape with the development of quantum theories describing optical coherence and field states by Glauber in 1963[8]. Quantum Optics provides a robust framework for describing optical phenomena such as spontaneous emission, single-photon interference, Bose-Einstein statistics, etc.

In the following sections, we will briefly explore the process of quantizing an electromagnetic field from Maxwell's equations using appropriate gauge transformations. The information presented in this and upcoming sections draws inspiration from 'The Quantum Theory of Light' by Loudon[1].

## 1.3 Quantum Theory of Light

As explained in earlier sections, a semiclassical theory involves solving a problem using classical  $\vec{E}$  and  $\vec{B}$  fields, while the atoms are described using quantum mechanics. This approach has proven highly successful in elucidating a vast array of optical experiments. However, despite its extensive historical application in optics, semiclassical theory encounters limitations when attempting to explain certain phenomena, thereby restricting its utility and reliability.

Our perspective aligns with the belief that quantum mechanics offers the most accurate predictions for measured quantities. In cases where semiclassical theory diverges from the results predicted by quantum mechanics for the same problem, we consider the semiclassical approach less reliable.

A complete quantum theory provides a more coherent framework that treats the entire system of fields and atoms in quantum mechanical terms. This necessitates the definition of operators for the physical observables associated with the  $\vec{E}$  and  $\vec{B}$  fields.

$$\vec{E} \rightarrow \hat{E} \quad , \quad \vec{B} \rightarrow \hat{B} \tag{1.1}$$

Note that  $\hat{E}$  and  $\hat{B}$  are no longer just algebraic variables, they are operators which do not necessarily commute with each other as we will find out in the upcoming sections.

## 1.4 Quantization of Electromagnetic Field

The  $\vec{E}$  and  $\vec{B}$  fields are governed by Maxwell's equations, forming the basis for both classical and quantum theories. The pivotal step in transitioning from classical to quantum

theory involves adopting the framework of a classical harmonic oscillator and transforming it into its quantum mechanical counterpart. Therefore, the current set of Maxwell's equations needs to be reformulated to exhibit harmonic oscillator behavior, and the subsequent transformation follows the prescribed conversion. To recap, the microscopic version of Maxwell's equations is stated as follows:

$$\vec{\nabla} \cdot \vec{E} = \frac{\rho}{\epsilon_0} \quad \text{Gauss's Law} \quad (1.2)$$

$$\vec{\nabla} \cdot \vec{B} = 0 \quad (1.3)$$

$$\vec{\nabla} \times \vec{E} = -\frac{\partial \vec{B}}{\partial t} \quad \text{Faraday's Law of Induction} \quad (1.4)$$

$$\vec{\nabla} \times \vec{B} = \mu_0 \left( \epsilon_0 \frac{\partial \vec{E}}{\partial t} + \vec{J} \right) \quad \text{Ampere's Circuital Law} \quad (1.5)$$

Here,  $\rho$  and  $\vec{J}$  denote the charge and current densities, respectively. To streamline the quantization process, we represent Maxwell's equations in terms of scalar and vector potentials, denoted as  $\phi$  and  $\vec{A}$ . Once the scalar and vector potentials are known, they can be utilized to determine the electric and magnetic fields as per the equations provided below:

$$\vec{B} = \vec{\nabla} \times \vec{A} \quad (1.6)$$

$$\vec{E} = -\vec{\nabla}\phi - \frac{\partial \vec{A}}{\partial t} \quad (1.7)$$

A noteworthy property of these potentials is that they can undergo transformations through a set of gauge transformations while leaving the electric and magnetic fields invariant under these transformations.

$$\vec{A} = \vec{A}' - \vec{\nabla}\chi \quad (1.8)$$

$$\phi = \phi' + \frac{\partial \chi}{\partial t} \quad (1.9)$$

Here,  $\chi$  is an arbitrary function  $\chi(\vec{r}, t)$  of position and time, also referred to as the gauge function. The fundamental concept behind this transformation is to choose a gauge, or a specific  $\chi$ , that simplifies the solutions to the complex equations derived from substituting  $\vec{A}$  and  $\chi$  into Maxwell's equations. A specific gauge choice that renders the divergence of  $\vec{A}$  zero is known as the Coulomb gauge. Adopting the Coulomb gauge simplifies the field equations, which now take the form:

$$-\nabla^2 \vec{A} + \frac{1}{c^2} \frac{\partial \vec{\nabla}\phi}{\partial t} + \frac{1}{c^2} \frac{\partial^2 \vec{A}}{\partial t^2} = 0 \quad (1.10)$$

$$-\nabla^2 \phi = \frac{\rho}{\epsilon_0} \quad (1.11)$$

The equation related to the scalar potential is essentially the Poisson's equation, and its solution is already known. However, the equation expressed in terms of the vector potential remains intricate and requires some effort to achieve the desired form. According to the Helmholtz theorem, any vector field can be expressed in terms of its solenoidal (transverse) and irrotational (longitudinal) components.

$$\vec{A} = \vec{A}_T + \vec{A}_L \quad (1.12)$$

$$\vec{\nabla} \cdot \vec{A}_T = 0 \quad (1.13)$$

$$\vec{\nabla} \times \vec{A}_L = 0 \quad (1.14)$$

Utilizing the aforementioned definitions in conjunction with the Coulomb gauge condition, we can bifurcate the Maxwell's equations and field equations into two distinct sets.

$$-\vec{\nabla}^2 \vec{A} + \frac{1}{c^2} \frac{\partial^2 \vec{A}}{\partial t^2} = \mu_0 \vec{J}_T \quad (1.15) \quad \frac{1}{c^2} \frac{\partial \vec{\nabla} \phi}{\partial t} = \mu_0 \vec{J}_L \quad (1.16)$$

Maxwell's Equations in Transverse form:

$$\vec{\nabla} \times \vec{E}_T = -\frac{\partial \vec{B}_T}{\partial t} \quad (1.17) \quad \vec{\nabla} \times \vec{B}_T = \mu_0 \epsilon_0 \frac{\partial \vec{E}_T}{\partial t} + \mu_0 \vec{J}_T \quad (1.19)$$

$$\vec{\nabla} \cdot \vec{E}_T = 0 \quad (1.18) \quad \vec{\nabla} \cdot \vec{B}_T = 0 \quad (1.20)$$

Maxwell's Equations in Longitudinal form:

$$\vec{\nabla} \cdot \vec{E}_L = \frac{\rho}{\epsilon_0} \quad (1.21)$$

We now focus on the solution for free fields, implying that the field exists in a region of space where  $\vec{J}_T = 0$ . Consequently, the field equation (1.15) undergoes transformation to:

$$-\vec{\nabla}^2 \vec{A} + \frac{1}{c^2} \frac{\partial^2 \vec{A}}{\partial t^2} = 0 \quad (1.22)$$

We assume standing wave solutions with periodic boundary conditions inside a region of space known as the quantization cavity. Utilizing these assumptions, we can express the vector potential as a sum of contributions from the modes of the cavity. Each mode is uniquely labeled by its wave propagation vector  $\mathbf{k}$  and the polarization  $\lambda$ .

$$\sum_k \sum_{\lambda=1,2} \vec{e}_{k\lambda} A_{k\lambda}(r, t) \quad (1.23)$$

Where  $\vec{e}_{k\lambda}$  represents the two orthogonal polarizations of each mode, and  $A_{k\lambda}(r, t)$  can be further decomposed into the product of time-independent modal coefficients and plane waves, as follows:

$$A_{k\lambda}(r, t) = A_{k\lambda}(t) e^{ik \cdot r} + A_{k\lambda}^*(t) e^{-ik \cdot r} \quad (1.24)$$

$$\vec{e}_{k\lambda} \cdot \vec{e}_{k\lambda'} = \delta_{\lambda, \lambda'} \quad (1.25)$$

The modal coefficients defined above are independent of each other, and each one individually satisfies the field equation (1.22).

$$k^2 A_{k\lambda}(t) + \frac{1}{c^2} \frac{\partial^2 A_{k\lambda}(t)}{\partial t^2} = 0 \quad (1.26)$$

If we substitute  $\omega_k = ck$  and rewrite the equation, we immediately recognize it as that of a harmonic oscillator, with  $\omega_k$  being the angular frequency of the oscillator. Finally, we arrive at a point from which we can delve into the quantum theory by calculating field energy and introducing field operators.

$$\frac{\partial^2 A_{k\lambda}(t)}{\partial t^2} + \omega_k^2 A_{k\lambda}(t) = 0 \quad (1.27)$$

The solution to the above equation can be taken in the form  $A_{k\lambda}(t) = A_{k\lambda} e^{-i\omega_k t}$ , and thus, the modal coefficients finally take the following form.

$$A_{k\lambda}(r, t) = A_{k\lambda} \exp(-i\omega_k t + ik \cdot r) + A_{k\lambda}^*(t) \exp(i\omega_k t - ik \cdot r) \quad (1.28)$$

We compute the electric and magnetic fields from the vector potentials using the transverse form of equations (1.6) and (1.7).

$$\vec{E}(r, t) = \sum_k \sum_{\lambda=1,2} \vec{e}_{k\lambda} E_{k\lambda}(r, t) \quad (1.29)$$

where

$$E_{k\lambda}(r, t) = i\omega_k [A_{k\lambda} e^{-i\omega_k t + ik \cdot r} + A_{k\lambda}^*(t) e^{i\omega_k t - ik \cdot r}] \quad (1.30)$$

Similarly for the magnetic field,

$$\vec{B}(r, t) = \sum_k \sum_{\lambda=1,2} \frac{k \times \vec{e}_{k\lambda}}{|k|} B_{k\lambda}(r, t) \quad (1.31)$$

where

$$B_{k\lambda}(r, t) = ik [A_{k\lambda} e^{-i\omega_k t + ik \cdot r} + A_{k\lambda}^*(t) e^{i\omega_k t - ik \cdot r}] \quad (1.32)$$

To determine the energy of an electromagnetic field, we substitute the above definitions of electric and magnetic fields into the energy density and integrate over the space within the cavity.

$$\mathcal{E} = 1/2 \int_{cavity} \left[ \epsilon_0 \vec{E}(r, t) \cdot \vec{E}(r, t) + \frac{\vec{B}(r, t) \cdot \vec{B}(r, t)}{\mu_0} \right] dV \quad (1.33)$$

After some algebraic manipulations, we arrive at a form for the energy that consists of the sum of time-independent contributions from individual modes.

$$\mathcal{E} = \sum_k \sum_{\lambda=1,2} \mathcal{E}_{k\lambda} \quad (1.34)$$

with

$$\mathcal{E}_{k\lambda} = \epsilon_0 V \omega_k^2 (A_{k\lambda} A_{k\lambda}^* + A_{k\lambda}^* A_{k\lambda}) \quad (1.35)$$

We will now review some key aspects of a one-dimensional **Quantum Harmonic Oscillator** defined on phase space operators  $(\hat{q}, \hat{p})$ .

$$\hat{\mathcal{H}} = \frac{\hat{p}^2}{2m} + \frac{m\omega^2 \hat{q}^2}{2} \quad (1.36)$$

It is convenient to express the generalized position and its conjugate momentum operator in terms of dimensionless creation and destruction operators.

$$\hat{a} = \frac{1}{\sqrt{2m\hbar\omega}} (m\omega\hat{q} + i\hat{p}) \quad , \quad \hat{a}^\dagger = \frac{1}{\sqrt{2m\hbar\omega}} (m\omega\hat{q} - i\hat{p}) \quad (1.37)$$

$$[\hat{q}, \hat{p}] = i\hbar \quad , \quad [\hat{a}, \hat{a}^\dagger] = 1 \quad (1.38)$$

The creation and annihilation operators are non-hermitian and do not represent any physical observable. However, the product  $\hat{\mathcal{N}}^\dagger = \hat{a}^\dagger \hat{a}$  represents the number operator and shares a common eigenbasis  $|n\rangle$  with the Hamiltonian. The creation and annihilation operators are also termed as ladder operators as they raise and lower the energy eigenvalue of an energy eigenstate by a quantum of energy  $\hbar\omega$  respectively. The eigenvalue equation is:

$$\hat{\mathcal{H}} |n\rangle = \hbar\omega (\hat{a}^\dagger \hat{a} + 1/2) |n\rangle = E_n |n\rangle \quad (1.39)$$

$$\hat{a} |n\rangle = \sqrt{n} |n-1\rangle \quad , \quad \hat{a}^\dagger |n\rangle = \sqrt{n+1} |n+1\rangle \quad (1.40)$$

$$\hat{\mathcal{H}} |n\rangle = \frac{1}{2} \hbar\omega (\hat{a} \hat{a}^\dagger + \hat{a}^\dagger \hat{a}) |n\rangle \quad (1.41)$$

The Hamiltonian written in this form is similar to the one in (1.35), providing a key link from which we can transition from the classical field vector to the field operator  $\vec{A} \rightarrow \hat{A}$  by defining it using the creation and annihilation operators. A quantum harmonic oscillator



is associated with each mode  $k\lambda$  of the radiation field in the quantization cavity. Thus, we add an extra label  $k\lambda$  to the creation and annihilation operators, and now they are responsible for creating or destroying one photon of energy  $\hbar\omega_k$  respectively in each mode.

The state of a mode is spanned by an orthonormal eigenbasis  $|n_{k\lambda}\rangle$ , also called the Fock basis. The number operator  $\hat{\mathcal{N}} = \hat{a}_{k\lambda}^\dagger \hat{a}_{k\lambda}$  acting upon a Fock state gives an eigenvalue  $n_{k\lambda}$  equal to the number of photons in the corresponding cavity mode.

$$\hat{n}_{k\lambda} |n_{k\lambda}\rangle = \hat{a}_{k\lambda}^\dagger \hat{a}_{k\lambda} |n_{k\lambda}\rangle = n_{k\lambda} |n_{k\lambda}\rangle \quad (1.42)$$

$$\hat{a}_{k\lambda} |n_{k\lambda}\rangle = \sqrt{n_{k\lambda}} |n_{k\lambda} - 1\rangle \quad , \quad \hat{a}_{k\lambda}^\dagger |n_{k\lambda}\rangle = \sqrt{n_{k\lambda} + 1} |n_{k\lambda} + 1\rangle \quad (1.43)$$

The modes of the electromagnetic field are independent, and as a result, the operators labeled by different  $k\lambda$  commute with each other, giving rise to a generalized commutator relation:

$$\left[ \hat{a}_{k\lambda}, \hat{a}_{k'\lambda'}^\dagger \right] = \delta_{k,k'} \delta_{\lambda\lambda'} \quad (1.44)$$

The state of an electromagnetic field is the tensor product of states of the individual modes, which could be infinite and the Hamiltonian of such a field is the sum of Hamiltonian of all contributing modes.

$$\hat{\mathcal{H}} = \sum_k \sum_{\lambda=1,2} \hat{\mathcal{H}}_{k\lambda} \quad \text{where} \quad \hat{\mathcal{H}}_{k\lambda} = \frac{1}{2} \hbar \omega_k \left( \hat{a}_{k\lambda} \hat{a}_{k\lambda}^\dagger + \hat{a}_{k\lambda}^\dagger \hat{a}_{k\lambda} \right) \quad (1.45)$$

A simple comparison with equation (1.35) yields an expression for converting the classical vector potential amplitudes into their corresponding operator.

$$A_{k\lambda} \rightarrow \sqrt{\frac{\hbar}{2\epsilon_0 V \omega_k}} \hat{a}_{k\lambda} \quad \text{and} \quad A_{k\lambda}^* \rightarrow \sqrt{\frac{\hbar}{2\epsilon_0 V \omega_k}} \hat{a}_{k\lambda}^\dagger \quad (1.46)$$

We obtain the operator corresponding to the vector field  $\vec{A}$  by substituting the above values into equation (1.28).

$$\hat{A}(r, t) = \sum_k \sum_{\lambda=1,2} \sqrt{\frac{\hbar}{2\epsilon_0 V \omega_k}} \vec{e}_{k\lambda} \left[ \hat{a}_{k\lambda} e^{-i\omega_k t + i\mathbf{k}\cdot\mathbf{r}} + \hat{a}_{k\lambda}^\dagger e^{i\omega_k t - i\mathbf{k}\cdot\mathbf{r}} \right] \quad (1.47)$$

Similarly, we can determine the operators corresponding to the electric and magnetic fields by substituting the above definition of  $\hat{A}$  into the transverse forms of equations (1.6) and (1.7). In the calculations, a phase factor  $\chi_k(r, t) = \omega_k t - \mathbf{k} \cdot \mathbf{r} - \pi/2$  is introduced to simplify the expression.

$$\hat{E}(r, t) = \sum_k \sum_{\lambda=1,2} \sqrt{\frac{\hbar \omega_k}{2\epsilon_0 V}} \vec{e}_{k\lambda} \left[ \hat{a}_{k\lambda} e^{-i\chi_k(r,t)} + \hat{a}_{k\lambda}^\dagger e^{i\chi_k(r,t)} \right] \quad (1.48)$$

$$\hat{B}(r, t) = \sum_k \sum_{\lambda=1,2} \sqrt{\frac{\hbar}{2\epsilon_0 V \omega_k}} k \times \vec{e}_{k\lambda} \left[ \hat{a}_{k\lambda} e^{-iX_k(r,t)} + \hat{a}_{k\lambda}^\dagger e^{iX_k(r,t)} \right] \quad (1.49)$$

The above electric and magnetic field operators are Hermitian, representing physical observables as required by the postulates of Quantum Mechanics. In the above discussion, we focused on Number or Fock states of light. However, there are various other classes of standard states, such as coherent states, squeezed states, thermal states, and some exotic states like cat states, that have extensive applications in quantum optics experiments. In the upcoming section, we will delve into some of these states, shedding light on them, which will greatly enhance our understanding of Boson Sampling.

## 1.5 States in Quantum Mechanics

According to the first postulate of Quantum Mechanics as described in [9], any isolated physical system is associated with a Hilbert space, also known as the state space of the system and we can completely describe this system by a state vector which resides in this Hilbert space. Alternatively, We can also use the concept of a density matrix or a density operator, which is mathematically equivalent to the state vector approach, in the formulation of Quantum Mechanics.

In the realm of Quantum Computing, we frequently encounter states existing within a two-dimensional state-space, which is defined by an orthonormal basis  $\{|0\rangle, |1\rangle\}$ .

$$|\psi\rangle = a|0\rangle + b|1\rangle \quad (1.50)$$

In order for the state to be normalizable, the complex numbers  $a$  and  $b$  must satisfy the condition  $|a|^2 + |b|^2 = 1$ .

### 1.5.1 Pure States

A state of a quantum system, denoted by  $|\psi\rangle$ , that is known exactly is referred to as a *pure state*. The density matrix of such states are simply given by:

$$\rho = |\psi\rangle \langle\psi| \quad (1.51)$$

and it satisfies the following property:

$$\text{tr}(\rho^2) = 1 \quad (1.52)$$

### 1.5.2 Mixed States

On the other hand, A *mixed state* is said to be a mixture of different *pure states* in the ensemble of  $\rho$ . The density matrix of such states are described as below:

$$\rho = \sum_i p_i |\psi_i\rangle \langle \psi_i| \quad (1.53)$$

We refer to  $\{p_i, |\psi_i\rangle\}$  as an ensemble of pure states, where  $p_i$  are the respective probabilities of being in one of the states  $\{|\psi_i\rangle\}$  and the density matrix of any mixed state satisfies the following property:

$$\text{tr}(\rho^2) < 1 \quad (1.54)$$

The concept of mixture comes into play when we introduce noise into our quantum system, leading to an introduction of ignorance into our knowledge of the quantum state.

## 1.6 Single Mode States

In the context of Quantum Optics, we will now shift our focus to single-mode excitations of the electromagnetic field. The reliability of a classical theory is determined by its agreement with its quantum counterpart in predicting phenomena. There is a crucial classification of excitations of the electromagnetic field based on this fundamental difference.

A classical state of light, such as coherent or chaotic light, when used in experiments, yields the same predictions as that of classical theory. On the contrary, there is a class of states termed as non-classical states of light that deviate from the predictions of classical theories. The coherence properties and fluctuations of a non-classical light beam cannot be explained using classical terms. It is also stated that when a state of light diverges from classicality, it exhibits quantumness.

Various parameters, such as Mandel's parameter and squeezing parameter, help measure and classify the quantum nature of fluctuations in a light beam. We will now delve into understanding the most important states of single-mode light in Quantum Optics.

### 1.6.1 Fock States

Fock states, or Number states, are the eigenstates of the number operator  $\mathcal{N} = \hat{a}^\dagger \hat{a}$ , which commute with the Hamiltonian, and hence, they are also referred to as the energy eigenstates.

$$\hat{\mathcal{H}} |n\rangle = \hbar\omega (\hat{a}^\dagger \hat{a} + 1/2) |n\rangle = E_n |n\rangle \quad (1.55)$$

The uncertainty of photon number associated with the number states  $(\Delta n)^2 = 0$ , indicating that a Fock state of light is expected to have exactly  $n$  number of photon excitations. In terms of quadrature operators, the eigenvalue equation can be reformulated as follows:

$$\left(\hat{X}^2 + \hat{Y}^2\right) |n\rangle = \left(n + \frac{1}{2}\right) |n\rangle \quad (1.56)$$

The expectation values and uncertainties associated with quadratures in a number state can be expressed as follows:

$$\langle n | \hat{X} | n \rangle = \langle n | \hat{Y} | n \rangle = 0 \quad (1.57)$$

$$(\Delta X)^2 = (\Delta Y)^2 = \frac{1}{2} \left( n + \frac{1}{2} \right) \quad (1.58)$$

Hence, we can observe that the quadratures X and Y in number states have identical properties to the vacuum state  $|0\rangle$ , being the state with minimum uncertainty in quadratures.

### 1.6.2 Coherent States

Coherent states are the most commonly used states of light in optics experiments. The properties of coherent states resemble those of a classical electromagnetic wave. In fact, a single-mode laser generates such a state of light when operated well above the threshold. A coherent state of light is denoted as  $|\alpha\rangle$  with  $\alpha \in \mathbb{C}$ . It might be tempting to believe that a coherent state is just a number state with a different parameter, which is very misleading. The construction of coherent states is fundamentally different, and their key property is that they are the eigenstates of the annihilation operator of the mode. Furthermore, a coherent state can be expressed as a linear superposition of number states.

$$\hat{a} |\alpha\rangle = \alpha |\alpha\rangle \quad (1.59)$$

$$|\alpha\rangle = e^{-\frac{|\alpha|^2}{2}} \sum_n \frac{\alpha^n}{\sqrt{n!}} |n\rangle \quad (1.60)$$

There is a very elegant mathematical tool called the displacement operator that aids in generating coherent states from vacuum states. Displacement operators possess interesting properties that will be highly useful in the theory of Boson Sampling. Let's outline some of those properties for better understanding.

$$|\alpha\rangle = \hat{D}(\alpha) |0\rangle \quad (1.61)$$

with the unitary displacement operator being defined as

$$\hat{D}(\alpha) = \exp(\alpha \hat{a}^\dagger - \alpha^* \hat{a}) \quad (1.62)$$

It is named a displacement operator for several reasons, one of them being that by operating it on the annihilation operator, it displaces it by an amount of  $\alpha$ .

$$\hat{D}^\dagger(\alpha) \hat{a} \hat{D}(\alpha) = \hat{a} + \alpha \quad (1.63)$$

and

$$\hat{D}^\dagger(\alpha) \hat{a}^\dagger \hat{D}(\alpha) = \hat{a}^\dagger + \alpha^* \quad (1.64)$$

The photon number expectation value and its associated uncertainty in a coherent state can be calculated quite easily using the properties of creation and annihilation operators, and are presented as follows:

$$\langle \hat{n} \rangle = \langle \alpha | \hat{a}^\dagger \hat{a} | \alpha \rangle = |\alpha|^2 \quad (1.65)$$

and the variance in photon number is given by

$$(\Delta \hat{n})^2 = |\alpha|^2 \quad (1.66)$$

Similarly, the quadrature expectation values can be calculated as follows:

$$\langle \hat{X} \rangle = \frac{1}{2} \langle \alpha | \hat{a}^\dagger + \hat{a} | \alpha \rangle = \frac{1}{2} (\alpha + \alpha^*) = |\alpha| \cos \theta \quad (1.67)$$

$$\langle \hat{Y} \rangle = \frac{1}{2} \langle \alpha | \hat{a} - \hat{a}^\dagger | \alpha \rangle = \frac{1}{2} (\alpha - \alpha^*) = |\alpha| \sin \theta \quad (1.68)$$

After performing the calculations, we can observe that the quadrature variances are:

$$(\Delta \hat{X})^2 = (\Delta \hat{Y})^2 = \frac{1}{4} \quad (1.69)$$

Hence, it is evident that a coherent state is a minimum quadrature uncertainty state, irrespective of its average photon number.

### 1.6.3 Squeezed States

The introduction of squeezing aims to reduce the uncertainties of fields along certain phase angles, albeit at the expense of increasing uncertainties along perpendicular angles. Such field excitations are termed quadrature squeezed states. Squeezed states constitute a highly significant class, showcasing non-classical characteristics and finding extensive applications in interferometric experiments where precision is critical, as exemplified in the detection of gravitational waves in LIGO.

#### 1.6.3.1 Squeezed Vacuum States

Similar to the construction of a coherent state by displacing the vacuum state with a unitary displacement operator, squeezed vacuum states are prepared by applying a unitary squeezing operator to the vacuum state.

$$|\zeta\rangle = \hat{S}(\zeta) |0\rangle \quad , \quad \zeta \in \mathbb{C} \quad (1.70)$$

where the squeezing operator is defined as

$$\hat{S}(\zeta) = \exp\left(\frac{\zeta^* (\hat{a})^2}{2} - \frac{\zeta (\hat{a}^\dagger)^2}{2}\right) \quad (1.71)$$

Due to the quadratic expression of creation and annihilation operators, it can be deduced that the squeezed vacuum states are a linear superposition of even-number states. After a bit of calculation, we can express their exact form as follows:

$$|\zeta\rangle = \sqrt{\text{sech } r} \sum_n \frac{\sqrt{(2n)!}}{n!} \left( \frac{-\exp(i\phi) \tanh r}{2} \right)^n |2n\rangle \quad (1.72)$$

The photon number expectation value in a squeezed vacuum state is given by:

$$\langle \hat{n} \rangle = \langle \zeta | \hat{a}^\dagger \hat{a} | \zeta \rangle = \sinh^2 r \quad (1.73)$$

and the variance of photon number is given by:

$$(\Delta \hat{n})^2 = 2 \sinh^4 r + 2 \sinh^2 r \quad (1.74)$$

Similarly, for quadratures, we can calculate the expectation value and variance. Utilizing the fact that squeezed vacuum states are linear superposition of even-numbered states, the expectation value of ladder operators or any linear combination of them is going to be zero.

$$\langle \hat{X} \rangle = \frac{1}{2} \langle \zeta | \hat{a} + \hat{a}^\dagger | \zeta \rangle = 0 \quad (1.75)$$

$$\langle \hat{Y} \rangle = \frac{1}{2} \langle \zeta | \hat{a} - \hat{a}^\dagger | \zeta \rangle = 0 \quad (1.76)$$

and

$$(\Delta \hat{X})^2 = \frac{1}{4} [e^{2r} \sin^2 \left( \frac{\phi}{2} \right) + e^{-2r} \cos^2 \left( \frac{\phi}{2} \right)] \quad (1.77)$$

$$(\Delta \hat{Y})^2 = \frac{1}{4} [e^{2r} \cos^2 \left( \frac{\phi}{2} \right) + e^{-2r} \sin^2 \left( \frac{\phi}{2} \right)] \quad (1.78)$$

It can be observed that the variances of quadratures depend on the phase angle. When plotting a curve against X and Y quadratures, we obtain an ellipse centered at the origin, inclined at an angle  $\phi/2$  with the axes. These curves vividly demonstrate the concept of squeezing one quadrature at the cost of expanding the one perpendicular to it.

### 1.6.3.2 Displaced Squeezed States

The primary motivation for introducing squeezed coherent states is to address the limitation of squeezed vacuum states in serving as carriers of information in systems that employ homodyne detection. We obtain a squeezed coherent state by initially applying the squeezing operator followed by the displacement operator. An equivalent representation, where the order of operators is reversed, is also possible, but we will not delve into the details of that topic.

$$|\alpha, \zeta\rangle = \hat{D}(\alpha) \hat{S}(\zeta) |0\rangle \quad (1.79)$$

Expanding squeezed coherent states involves a somewhat intricate calculation but can be accomplished using the existing properties of the mode operators used so far. To estimate the expectation values and variance of photon number and quadratures, it is essential to outline some important properties of the unitary transform of the creation and annihilation operators.

$$\hat{S}^\dagger(\zeta) \hat{D}^\dagger(\alpha) \hat{a} \hat{D}(\alpha) \hat{S}(\zeta) = \hat{a} \cosh r - \hat{a}^\dagger e^{i\phi} \sinh r + \alpha \quad (1.80)$$

$$\hat{S}^\dagger(\zeta) \hat{D}^\dagger(\alpha) \hat{a}^\dagger \hat{D}(\alpha) \hat{S}(\zeta) = \hat{a}^\dagger \cosh r - \hat{a} e^{-i\phi} \sinh r + \alpha^* \quad (1.81)$$

The above definitions of transforms assist in simplifying the expressions for the mean and variance of photon number and quadratures. Upon performing the calculations, we arrive at the following results:

$$\langle \hat{n} \rangle = |\alpha|^2 + \sinh^2 r \quad (1.82)$$

and variance in photon number

$$(\Delta \hat{n})^2 = |\alpha|^2 \left\{ e^{2r} \sin^2 \left( \theta - \frac{\phi}{2} \right) + e^{-2r} \cos^2 \left( \theta - \frac{\phi}{2} \right) \right\} + 2 \sinh^2 r (\sinh^2 r + 1) \quad (1.83)$$

Similarly, for quadratures, it is straightforward to deduce from the previous results:

$$\langle \hat{X} \rangle = \frac{1}{2} \langle \alpha, \zeta | \hat{a} + \hat{a}^\dagger | \alpha, \zeta \rangle = |\alpha| \cos \theta \quad (1.84)$$

$$\langle \hat{Y} \rangle = \frac{1}{2} \langle \alpha, \zeta | \hat{a} - \hat{a}^\dagger | \alpha, \zeta \rangle = |\alpha| \sin \theta \quad (1.85)$$

and

$$(\Delta \hat{X})^2 = \frac{1}{4} \left[ e^{2r} \sin^2 \left( \frac{\phi}{2} \right) + e^{-2r} \cos^2 \left( \frac{\phi}{2} \right) \right] \quad (1.86)$$

$$(\Delta \hat{Y})^2 = \frac{1}{4} \left[ e^{2r} \cos^2 \left( \frac{\phi}{2} \right) + e^{-2r} \sin^2 \left( \frac{\phi}{2} \right) \right] \quad (1.87)$$

We can observe that the profile of the squeezing is merely displaced by an amount  $\alpha$ . Graphically, it can be visualized as the same curve obtained in the squeezed vacuum state, but now it is displaced to the center  $\alpha$ . This is also reflected in the above results, as the variances of quadratures remain unaffected, but their means are now pointing at the point  $\alpha$ .

### 1.6.4 Thermal States

A thermal state describes the state of thermal equilibrium of a single mode with a thermal bath. In fact, thermal states aptly describe the radiation of many other chaotic sources of light. An important point to note is that all the previously studied states were pure states, whereas thermal states are mixed states. For such states, we describe the state of light in terms of a density matrix.

$$\rho_{th} = \sum_n P(n) |n\rangle \langle n| \quad (1.88)$$

Where  $P(n)$  is the probability distribution and its form as given below is derived from a geometrical distribution. Here  $\bar{n}$  is another term used for the mean photon number in the state.

$$P(n) = \frac{\bar{n}^n}{(1 + \bar{n})^{1+n}} \quad (1.89)$$

Chaotic light states exhibit resemblance with number states in terms of quadrature properties. The corresponding expectation value and variance of quadratures are given below:

$$\langle \hat{X} \rangle = \sum_n P(n) \langle n | \hat{X} | n \rangle = 0 \quad (1.90)$$

$$\langle \hat{Y} \rangle = \sum_n P(n) \langle n | \hat{Y} | n \rangle = 0 \quad (1.91)$$

and

$$(\Delta \hat{X})^2 = \frac{1}{2} \left( \langle \hat{n} \rangle + \frac{1}{2} \right) \quad (1.92)$$

$$(\Delta \hat{Y})^2 = \frac{1}{2} \left( \langle \hat{n} \rangle + \frac{1}{2} \right) \quad (1.93)$$

We can notice that the quadrature calculations are actually similar to the ones we did in number states, just with  $n$  being replaced by the average photon number  $\langle \hat{n} \rangle$ .

## 1.7 Photon Interference at a Beam Splitter

Now that we have studied all the important single-mode states of an electromagnetic field, we will shift our focus to studying the interference between these states at a beam splitter. A beam splitter plays a crucial role in all interferometric experiments, and the simplest model of a beam splitter could be a half-silvered mirror or a partially reflecting interface between two glass prisms.



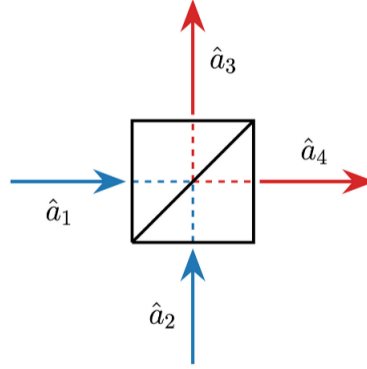


Figure 1.1: Beam Splitter, Source: <https://www.cantorsparadise.com/quantum-beam-splitters-the-hong-ou-mandel-effect-a59eda66de04>

This is a basic illustration illustrating the operational principles of a beam splitter within a quantum framework. The system involves two input modes, labeled as  $a_1$  and  $a_2$ , which undergo transformation to yield two output modes, labeled as  $a_3$  and  $a_4$ . A beam splitter facilitates a linear relationship between the input and output modes, and no optical mode either begins or ends at a beam splitter. The connection between the input and output modes is determined by the physical configuration of the beam splitter, specifically the transmittance and reflectance of the interface. Mathematically, this relationship can be expressed in terms of matrix components that encapsulate information about the transformation.

$$\begin{bmatrix} \hat{a}_4 \\ \hat{a}_3 \end{bmatrix} = \begin{bmatrix} t_1 & r_2 \\ r_1 & t_2 \end{bmatrix} \begin{bmatrix} \hat{a}_1 \\ \hat{a}_2 \end{bmatrix} \quad (1.94)$$

The  $2 \times 2$  matrix presented describes the configuration of a lossless unbalanced beam splitter. However, the elements of the matrix cannot be arbitrary; there are constraints imposed on them by the principle of conservation of energy. This principle dictates that the matrix must be unitary.

$$|t_1|^2 + |r_2|^2 = 1 \quad , \quad |t_2|^2 + |r_1|^2 = 1 \quad (1.95)$$

$$t_2^* r_2 + r_1^* t_1 = 0 \quad , \quad t_1^* r_1 + r_2^* t_2 = 0 \quad (1.96)$$

We can simplify the expression further by assuming a symmetry between the transmission and reflection coefficients concerning the exchange between  $a_1$  and  $a_2$ . This simplification results in  $|t_1| = |t_2| = t$  and  $|r_1| = |r_2| = r$ . Another implication of energy conservation is that if the input modes are orthonormal, then the corresponding output modes are also orthonormal.

If

$$[\hat{a}_1, \hat{a}_2^\dagger] = [\hat{a}_2, \hat{a}_1^\dagger] = 0 \quad , \quad [\hat{a}_1, \hat{a}_1^\dagger] = [\hat{a}_2, \hat{a}_2^\dagger] = 1 \quad (1.97)$$

From the relations (1.90) and (1.91), assuming symmetry between  $t$  and  $r$ , we can deduce the following equations:

$$\hat{a}_4 = t\hat{a}_1 + r\hat{a}_2 \quad , \quad \hat{a}_4^\dagger = t^*\hat{a}_1^\dagger + r^*\hat{a}_2^\dagger \quad (1.98)$$

$$\hat{a}_3 = t\hat{a}_2 + r\hat{a}_1 \quad , \quad \hat{a}_3^\dagger = t^*\hat{a}_2^\dagger + r^*\hat{a}_1^\dagger \quad (1.99)$$

$$|t|^2 + |r|^2 = 1 \quad , \quad rt^* + tr^* = 0 \quad (1.100)$$

which allows us to write:

$$[\hat{a}_3, \hat{a}_4^\dagger] = [\hat{a}_4, \hat{a}_3^\dagger] = 0 \quad , \quad [\hat{a}_3, \hat{a}_3^\dagger] = [\hat{a}_4, \hat{a}_4^\dagger] = 1 \quad (1.101)$$

With these relations, we can construct observables on output modes.

$$\hat{n}_{a_4} = \hat{a}_4^\dagger \hat{a}_4 = (t^*\hat{a}_1^\dagger + r^*\hat{a}_2^\dagger)(t\hat{a}_1 + r\hat{a}_2) = |t|^2\hat{n}_{a_1} + |r|^2\hat{n}_{a_2} + tr^*\hat{a}_2^\dagger\hat{a}_1 + rt^*\hat{a}_1^\dagger\hat{a}_2 \quad (1.102)$$

$$\hat{n}_{a_3} = \hat{a}_3^\dagger \hat{a}_3 = (t^*\hat{a}_2^\dagger + r^*\hat{a}_1^\dagger)(t\hat{a}_2 + r\hat{a}_1) = |t|^2\hat{n}_{a_2} + |r|^2\hat{n}_{a_1} + rt^*\hat{a}_2^\dagger\hat{a}_1 + tr^*\hat{a}_1^\dagger\hat{a}_2 \quad (1.103)$$

Similarly, we can construct field operators corresponding to  $a_3$  and  $a_4$  modes from the ones belonging to  $a_1$  and  $a_2$ . So far, we have dealt with a generalized lossless unbalanced beam splitter, but we can also impose additional restrictions on the elements to arrive at a balanced beam splitter, which evenly splits each input mode in a 50:50 ratio.

$$|r|^2 = |t|^2 = \frac{1}{2} \implies r = \frac{e^{i\phi_r}}{\sqrt{2}} \quad , \quad t = \frac{e^{i\phi_t}}{\sqrt{2}} \quad (1.104)$$

$$rt^* + tr^* = 0 \implies \phi_r = \phi_t \pm \frac{\pi}{2} \quad (1.105)$$

$$\begin{bmatrix} t & r \\ r & t \end{bmatrix} = \frac{e^{i\phi_t}}{\sqrt{2}} \begin{bmatrix} 1 & \pm i \\ \pm i & 1 \end{bmatrix} \quad (1.106)$$

A crucial point to note here is that the beam splitter matrix is represented as a unitary matrix. This understanding is essential for comprehending interferometers used in the Boson Sampling protocol, which are not limited to just 2 modes. A generalized interferometer is represented by an  $M \times M$  unitary matrix, transforming  $M$  input modes into  $M$  output modes. We will study this in detail in the next chapter, which formally introduces Boson Sampling.

---

## Boson Sampling

Quantum computers are constructed based on an architecture governed by the postulates of Quantum Mechanics, and they are anticipated to outperform classical computers significantly in terms of speed. The fundamental unit in a quantum computer is the quantum bit, or qubit. Unlike classical bits, a qubit can exist in any linear superposition of the states 0 and 1, allowing it to perform computations on both states simultaneously. Upon measurement in the computational basis, it probabilistically collapses to a specific result, akin to the collapse of a wavefunction to one of its eigenstates in Quantum Mechanics. This quantum speedup, compared to classical computers, is a crucial aspect in achieving what has been referred to as **Quantum Supremacy**.

For a quantum computer to be practically useful in solving real-world problems, a more extensive architecture is required, with elements that can be controlled coherently and are fault-tolerant. While there have been successful attempts to build quantum computers with multiple qubits in the industry, the realization of a scalable and universal quantum computer may still be several years away. Nonetheless, the field of Quantum Engineering is incredibly exciting, and one notable development in this area is Boson Sampling.

Boson Sampling, a non-universal quantum computation model, relies on linear optical networks and states of the electromagnetic field within the context of quantum optics. In this chapter, we will delve into the problem Boson Sampling addresses and explore several developed protocols in this domain.

### 2.1 Boson Sampling - The Model

The Boson Sampling model, as originally introduced by Aaronson and Arkhipov in [10], is a basic framework for optical quantum computing. It comprises single photon generators, a linear optical network, and photodetectors to measure the number of photons in the output modes.

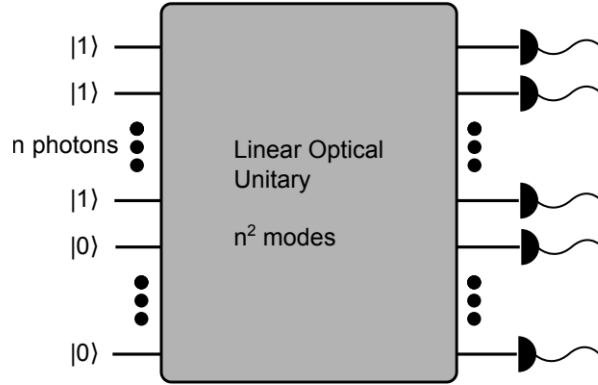


Figure 2.1: Boson Sampler, Source: [11]

Despite its simplicity, the authors demonstrated that such a device cannot be efficiently simulated by classical computers. Boson Sampling is a non-universal model of quantum computation, implying that it cannot solve all problems solvable by a Turing machine. The authors further demonstrated that the existence of a polynomial time classical algorithm capable of sampling from the exact or approximate probability distribution as an optical network's output would have significant implications for the polynomial hierarchy in complexity theory.

Before delving into the model, it's crucial to address the preference for Bosons over Fermions. Bosons and Fermions categorize particles based on their fundamental properties, with Bosons having integer spin (e.g., photons) and Fermions having half-integer spin (e.g., electrons, quarks). The rationale for choosing Bosons, as outlined in [10], lies in expressing the amplitude of  $n$  Boson processes in terms of permanents of  $n \times n$  matrices. Notably, problems involving permanents belong to the  $\#P$ -complete complexity class. On the other hand, the amplitude of  $n$  fermion processes can be expressed using determinants of  $n \times n$  matrices, falling into the  $P$  complexity class and allowing for efficient classical simulation. This distinction plays a pivotal role in the computational complexity of the Boson Sampling model.

The device/optical network as illustrated in the above figure, features  $m$  input modes through which  $n$  identical photons are transmitted, and  $m$  output modes where the output state is measured in the Fock basis. The input configuration can be any multimode state ket  $|s_1, \dots, s_m\rangle$  satisfying the conditions  $\sum_i s_i = n$  and  $s_1, \dots, s_m \geq 0$ . The nature of photons as Bosons allows them to occupy more than one in the same mode simultaneously, distinguishing them from Fermions. The basis states  $|S\rangle$  are defined as  $S \in \Phi_{m,n}$ , where  $\Phi_{m,n}$  is the set of tuples  $S = (s_1, \dots, s_m)$  satisfying the above conditions, and  $M = |\Phi_{m,n}|$  denotes the dimension of the Hilbert space in which the states exist. A simple permutation trick facilitates the calculation of the dimension  $M = \binom{m+n-1}{n}$ . Analogous to Quantum Mechanics, an arbitrary state ket can be expressed as a linear superposition of the base kets.

$$|\psi\rangle = \sum_{S \in \Phi_{m,n}} \beta_s |S\rangle \quad (2.1)$$

Here,  $\beta_s$  represents the complex coefficients, and when the state is normalized,  $\sum_{S \in \Phi_{m,n}} |\beta_s|^2 = 1$ . The Hilbert space corresponding to the set  $\Phi_{m,n}$  is denoted as  $H_{m,n}$ . Importantly, the Hilbert space in this model is not simply a tensor product of smaller Hilbert spaces. A standard convention for an input state, as followed in the paper by Aaronson and Arkhipov, is to feed the first  $n$  modes with 1 photon each, while the remaining channels are in the vacuum state:  $|1_n\rangle = |1, \dots, 1, 0, \dots, 0\rangle$ .

The input state is then evolved through a linear optical network represented by an  $m \times m$  unitary matrix  $U$ . The output of the system consists of samples from a distribution obtained after measuring the transformed state in the Fock basis. Any arbitrary unitary matrix can be decomposed into a product of elementary unitary matrices. Each of these elementary matrices represents an optical element that acts non-trivially on at most two modes and is the identity on the remaining  $m - 2$  modes. This decomposition was proven by Reck et al.[12]. The most commonly used optical elements are beam splitters and phase shifters. In other words, we can interpret this theorem to mean that any linear optical network could be constructed using beam splitters and phase shifters.

The probability distribution of output samples is related to the permanent of a submatrix of the original unitary matrix  $U$ . Before providing the exact expression, let's define the permanent of a matrix.

$$\text{Per} \begin{bmatrix} a & b \\ c & d \end{bmatrix} = ad + bc \quad (2.2)$$

And in general for  $n \times n$  matrices,

$$\text{Per}(X) = \sum_{\sigma \in S_n} \prod_{i=1}^n x_{i,\sigma(i)} \quad (2.3)$$

Where  $S_n$  represents the elements of the symmetry group of permutations of  $n$  elements. Now, let's define an output event  $\bar{n} = S = (n_1, n_2, \dots, n_m)$  which means that we want to find the probability of measuring  $n_1$  photons in mode 1,  $n_2$  photons in mode 2, and so on. The probability of such an event happening is then given by:

$$p(\bar{n}) = \frac{|\text{Per}(A_s)|^2}{n_1! n_2! \dots n_m!} \quad (2.4)$$

Where  $A_s$  is an  $n \times n$  submatrix obtained from the unitary  $U$  by keeping the first  $n$  columns, and row  $i$  is repeated  $n_i$  times. An important point to note is that the probability of each event occurring is related to the permanent of a different submatrix of the same unitary every time, which ensures its value being less than 1 and also the normalization

of the distribution. A common misconception that can be immediately discarded from the previous point is that Boson Sampling helps us calculate the permanent of a matrix, but it is not possible because to calculate the permanent, we might need an exponential number of runs as the space of output events also grows exponentially.

When considering the scenario of Exact Boson sampling, which involves precisely sampling from the actual probability distribution of photon interference pattern, we know that the calculation of the permanent of a complex matrix falls under the category of  $\#P$ -hard complexity class. This means that if there exists any classical algorithm that could efficiently sample from the exact distribution as that of a Boson sampler, it would imply a collapse in the polynomial hierarchy—a situation that is highly implausible in complexity theory.

Aaronson and Arkhipov also introduced the concept of Approximate Boson Sampling to approximate the permanent of matrices composed of random numbers from a complex normal distribution, up to an additive error represented by  $|GPE|_{\pm}^2$ . They utilized Stockmeyer’s algorithm to demonstrate that  $|GPE|_{\pm}^2$  is in  $BPP^{NP^{\mathcal{O}}}$ , where  $\mathcal{O}$  is an oracle that solves the approximate Boson Sampling problem. While it is known that a problem in  $BPP^{NP}$  is hard for classical algorithms, whether the approximate Boson Sampling problem is in  $\#P$  remains an open question. Nonetheless, the authors provide strong evidence supporting the  $\#P$  complexity of approximate Boson Sampling by relying on two conjectures.

First, the permanent-of-gaussians conjecture posits that estimating the permanent of a matrix up to a multiplicative error (denoted as  $GPE_x$ ) belongs to the  $\#P$  complexity class. Second, the permanent-anti-concentration conjecture implies a polynomial-time equivalence between  $GPE_x$  and  $|GPE|_{\pm}^2$ . Assuming these conjectures are true, it follows that  $P^{\#P} = BPP^{NP}$  unless Approximate Boson Sampling is in  $\#P$ .

### 2.1.1 Experimental Factors - AABS

A Boson Sampling device that surpasses the capabilities of a classical computer could provide evidence supporting the possibility of non-trivial quantum computation without the need for constructing a universal quantum computer. Demonstrating the superiority of a large Boson Sampling device would present a challenge to the Extended Church-Turing thesis. However, it’s important to note that, given the nature of complexity theory dealing with asymptotic statements, no single experiment is sufficient to disprove the Extended Church-Turing thesis.

One challenging aspect for experimentalists is to design an experiment with the right number of photons. This means that while a classical computer may struggle to sample from such a distribution, it should still be capable of verifying the results obtained from the Boson Sampler.

The experimental setup for Boson Sampling typically requires physical resources such as linear optical networks, photon sources and detectors as described in [10]. However, it

is worth noting that the experiment can also be conducted in a solid-state system using Bosonic excitations. The preparation of the standard input state ideally involves single-photon Fock states and vacuum states. Generating single photons can be challenging, but there are various techniques available for this purpose, as discussed in [13].

In the experimental setup, an interferometer is employed, represented by a unitary matrix. Once the unitary matrix is fixed, the number of beam splitters and phase shifters can be estimated using (Lemma 3.1) from Reck et al. [12]. This lemma provides a count of elements on the order of  $O(m^2)$ . However, scaling such an architecture with an increasing number of modes can be challenging. To address this issue, Aaronson and Arkhipov utilized a reduction technique. Since photons are present only in the first  $n$  out of  $m$  modes of the standard input state, they devised a way to parallelize the optical network. This modification allows the requirement on the number of optical elements to scale up to  $O(nm)$ , organized into only  $O(n \log m)$  layers.

The final step of the experiment involves measuring the transformed state in the Fock basis. This step requires  $m$  photon detectors with the capability of distinguishing the number of photons  $n_i$ . However, when  $m$  (total modes) is much larger than  $n$  (total photons), the probability of receiving more than one photon in any of the output modes is almost negligible, as demonstrated by the authors in "Boson Birthday Bound" [10]. Therefore, any bucket detector that clicks in the presence of a photon without giving an accurate information about the count of photons will be sufficient for the task of Boson Sampling. The main consideration here is the efficiency of such photodetectors, which has significantly improved over the decade. Higher efficiency enhances the scalability of such a setup.

What might go wrong? There are several potential sources of error that, if controlled more effectively, could reduce errors in the experiment. Some of the sources of error, as discussed in [10], include the low reliability of single photon Fock state generators, the inability of optical elements (such as beam splitters and phase shifters) to induce the desired unitary transformation, the network not being lossless, meaning photons could get lost along the way, the inefficiency of existing photodetectors, and the arrival of photons at photodetectors at different times due to a lack of calibration in optical fibers or a lack of synchronization among single photon sources. The last issue can result in distinguishable photons, and thus, the amplitudes will no longer be matrix permanents. Many of these challenges have been addressed in recent developments of Boson Sampling protocols, and we will explore some of them in the upcoming sections.

## 2.2 Scattershot Boson Sampling

We start this section by addressing the issues related to the unreliability of single-photon Fock state sources mentioned in the previous section. The current photon sources are not deterministic, and the probability of successfully generating the input state decreases

exponentially with an increase in  $n$ . With this motivation in mind, Lund et al [11] proposed an alternative scheme to generate the input state from Gaussian states of light. This is because there are better sources available that can deterministically produce non-classical states of light with a Gaussian Wigner function and high purity. The authors of this paper also investigate whether sampling from Gaussian states is still a computationally hard problem, introducing a new protocol called the Scattershot Boson Sampling protocol.

Instead of relying on single-photon Fock state sources, the authors introduced the idea of generating photons from two-mode squeezed states. The generation of two-mode squeezed states has traditionally been accomplished using spontaneous parametric down-conversion (SPDC) techniques. In the SPDC process, a strong pump beam is directed onto a nonlinear crystal, resulting in two modes: signal and idler. The output state is a two-mode squeezed vacuum, represented by the expression:

$$|\psi\rangle = \sqrt{1 - \chi^2} \sum_{p=0}^{\infty} \chi^p |p\rangle_1 |p\rangle_2 \quad (2.5)$$

Here  $0 \leq \chi < 1$  is the squeezing strength and the overall state is a gaussian state which can be produced quite reliably using this technique. The model of Boson Sampling from this setting, as described by the authors in [11], consists of  $2n^2$  optical modes, two-mode squeezed vacuum state sources (SPDC sources), a linear optical network with  $m = n^2$  modes, and photon-counting detectors. This allows the construction of an instance of the  $n$ -photon Boson Sampling problem. The idea is to input one mode from each of the  $n^2$  two-mode squeezed states into the interferometer, while the other one (herald mode) goes into a photon detector, as shown in the figure given below.

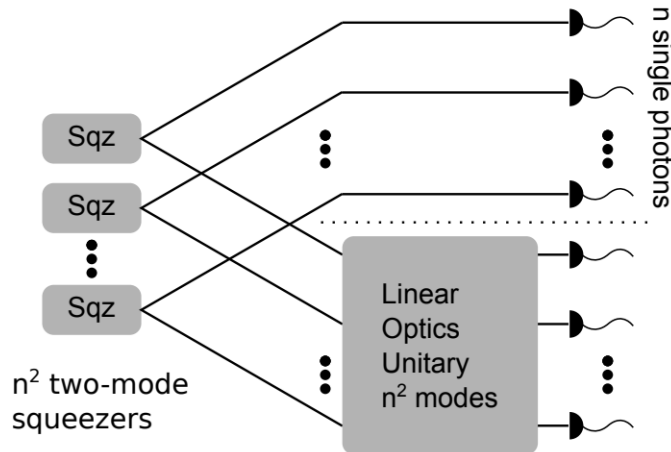


Figure 2.2: Scattershot Boson Sampler, Source:[11]

The total state of all modes before measurement in the Fock basis is given by a compact equation:



$$|\psi\rangle_{1,2} = U_j^{(2)} \prod_{h=1}^{n^2} \sqrt{1 - \chi^2} \sum_{p_h=0}^{\infty} \chi^{p_h} |p\rangle_{h1} |p\rangle_{h2} \quad (2.6)$$

The herald modes ( $h_1$ ) are not acted upon by the unitary and are used in the construction of the standard input states with  $n$  single photon Fock states and remaining vacuum states. Suppose that the arrangement of those 1 photons over herald modes is represented by a string  $k_h$ , then the state of the herald mode system can be written as:

$$|\phi\rangle_1 = \prod_{h=1}^{n^2} \left( \hat{a}_h^\dagger \right)^{k_h} |0\rangle_1 \quad (2.7)$$

Now partially tracing out the herald mode state over the total state of the system gives us:

$${}_1\langle\phi|\psi\rangle_{1,2} = U_j^{(2)} \prod_{h=1}^{n^2} \left( \hat{a}_h^\dagger \right)^{k_h} |0\rangle_2 \quad (2.8)$$

This equation represents an equivalence with an instance of Boson Sampling problem but with an additional dependency on the probabilistic behavior of the construction of the required input state, and the probability of detecting a particular arrangement  $k_h$  as calculated by the authors is given by  $\chi^{2n} (1 - \chi^2)^{n^2}$ . This probabilistic behavior introduces an additional exponential overhead to the Boson Sampling algorithm. Following the lines of argument in the paper[11], a rough proof (evidence) has been sketched by the authors to keep in order the fact that even with this exponential overhead, the problem still remains computationally hard to compute. Any existence of a classical algorithm that could efficiently sample from the exact probability distribution or even the approximate probability distribution would imply a collapse in the polynomial hierarchy, which is very unlikely.

The Scattershot Boson Sampling Protocol consists of non-adaptive linear optical networks, construction of two-mode squeezed states, and photon counting measurements. Such a device has the ability to efficiently solve a generalized Boson Sampling problem. Importantly, it remains a computationally hard problem for classical computers.

### 2.2.1 Experimental Factors - SBS

Experimenting with such a physical device comes with its own set of challenges. Constructing  $n^2$  identical two-mode squeezers, injecting them into a large optical network (which needs to be lossless), and dealing with the low efficiency of photodetectors are all significant hurdles in achieving accurate results. Recent efforts in this field aim to address these challenges, with approaches such as passive error correction against loss [14], time-multiplexed squeezed sources [15], and integrating squeezed state generators and optical networks on a single chip to reduce losses [16].

## 2.3 Gaussian Boson Sampling

In the previous exploration of the Scattershot Boson Sampling (SBS) protocol, it was observed that Gaussian states were used, but their Gaussian nature was eventually discarded by post-selecting on the herald modes to obtain single photons in a low-gain regime. With the aim of retaining the full Gaussian nature of the input states and reducing the size of the sampling space by a factor of  $\binom{N^2}{N}$  compared to the SBS protocol, C.Hamilton et al introduced a new Gaussian Boson Sampling (GBS) protocol in [17]. This protocol leverages the complete Gaussian nature of input states, allowing for operation in a high-gain regime. Additionally, it removes the constraint on using single-photon Fock input states, as seen in previous protocols.

The GBS protocol, as outlined in [17], involves a set of squeezed states passing through the linear interferometer and then being detected by the photon number detectors to measure the transformed state in the Fock basis. The paper also addresses the question of complexity, determining whether this sampling protocol, which uses Gaussian states instead of single-photon Fock states, remains a computationally hard problem. The authors provide evidence for the hardness of the problem and introduce a new theoretical formula to calculate the probability of obtaining an output photon pattern  $\bar{n}$  using a matrix function called the Hafnian.

The formulation of the sampling matrix in this protocol deviates slightly from that of previous versions of Boson Sampling. A notable feature is that the final sampling matrix absorbs characteristics from both the interferometer matrix and the covariance matrix representing the Gaussian input state. To comprehend this process, an understanding of the properties of the phase space representation in quantum optics is required. Additionally, it's essential to acknowledge that any M-mode Gaussian state can be represented using a  $2M \times 2M$  covariance matrix ( $\sigma$ ) and a  $2M$  displacement vector ( $d$ ), as given below:

$$\sigma_{ij} = \frac{1}{2} \langle \{ \hat{\zeta}_i, \hat{\zeta}_j \} \rangle - d_i d_j \quad , \quad d_j = \langle \hat{a}_j \rangle \quad (2.9)$$

The expression involves the operators  $\hat{\zeta}_j$ , which take the place of creation and annihilation operators  $\hat{a}_j$  and  $\hat{a}_j^\dagger$  for each mode  $j$ . Let's simplify the expression by assuming  $d_j = 0$ , and then we'll handle the case with non-zero displacement vectors. Using the methods in phase space representations of quantum states and operators [18], [19] and [20], we can formulate the probability of measuring  $\bar{n}$  as given below:

$$\Pr(\bar{n}) = \pi^M \int d^{2M} \alpha Q_{\hat{\rho}}(\alpha) P_{\bar{n}}(\alpha) \quad (2.10)$$

The  $Q_{\hat{\rho}}$  is the Q-function, or an alternate representation of the system state (density matrix  $\hat{\rho}$ ), and  $P_{\bar{n}}$  is the P-function corresponding to the measurement operator  $\hat{n}$ .

$$P_{\bar{n}}(\alpha) = \frac{e^{|\alpha|^2}}{n!} \left( \frac{\partial^2}{\partial \alpha \partial \alpha^*} \right)^n \delta(\alpha) \delta(\alpha^*) \quad \text{for } |n\rangle \langle n| \quad (2.11)$$

$$Q_{\hat{\rho}}(\alpha) = \frac{1}{\sqrt{|\pi\sigma_Q|}} e^{-\frac{1}{2}\alpha^\dagger \sigma_Q^{-1} \alpha} \quad (2.12)$$

Where  $\sigma_Q = \sigma + \mathbf{1}/2$ ,  $\alpha_\nu = [\alpha_1, \dots, \alpha_M, \alpha_1^*, \dots, \alpha_M^*]$ . Plugging these definitions into equation (2.10) followed by some analysis takes us to our desired equation for calculating the probability of obtaining an output pattern of photons  $\bar{n}$ .

$$\Pr(\bar{n}) = \frac{1}{\bar{n}! \sqrt{|\sigma_Q|}} \prod_{j=1}^M \left( \frac{\partial^2}{\partial \alpha_j \partial \alpha_j^*} \right)^{n_j} e^{\frac{1}{2} \alpha_\nu^t A \alpha_\nu} \Bigg|_{\alpha_\nu=0} \quad (2.13)$$

A represents the sampling matrix and is defined as given below:

$$A = \begin{bmatrix} 0 & \mathbf{1}_M \\ \mathbf{1}_M & 0 \end{bmatrix} [\mathbf{1}_{2M} - \sigma_Q^{-1}] \quad (2.14)$$

For simplicity, we will assume only 0 or 1 photon in the output mode, allowing us to define a 2M-dimensional vector, denoted as  $\mu$ , which records the position of the detected photon. For instance, if a photon is detected in the j-th mode, both the  $j^{th}$  and  $(M+j)^{th}$  entries of  $\mu$  will be activated. The expansion of 2N derivatives in Equation (2.11) results in a summation over all Perfect Matching Permutations (PMP) of the vector  $\mu$ .

$$\Pr(\bar{n}) = \frac{1}{\bar{n}! \sqrt{|\sigma_Q|}} \sum_{\mu' \in PMP} \prod_{j=1}^M A_{S_{\mu'_{(2j-1)}, \mu'_{(2j)}}} \quad (2.15)$$

Here,  $A_S$  represents a submatrix obtained by discarding the rows and columns corresponding to the 0 entries in the  $\mu$  vector. The summation over Perfect Matching Permutations (PMP) is equivalent to the Hafnian of the matrix, as defined by Caianiello in [21, 22]. This relationship allows us to finally connect the probability to the Hafnian of our sampling matrix.

$$\Pr(\bar{n}) = \frac{1}{\bar{n}! \sqrt{|\sigma|}} \text{Haf}(A_S) \quad (2.16)$$

The Hafnian of a matrix is a more general function than the permanent, and there exists a defined relationship between them, as given below:

$$\text{Per}(A) = \text{Haf} \left( \begin{bmatrix} 0 & A \\ A^t & 0 \end{bmatrix} \right) \quad (2.17)$$

Now, utilizing these definitions, let's delve into a detailed examination of the Gaussian Boson Sampling (GBS) protocol and its architecture. In this setup, we have K single-mode squeezed states (SMSS) as defined in (1.72), injected into an M-mode linear interferometer ( $K \leq M$ ). The interferometer is characterized by a Haar random unitary transformation,

described by an unitary matrix  $T$ . Subsequently, the state undergoes a transformation, and the resulting state at the end of the computation is measured in the Fock basis.

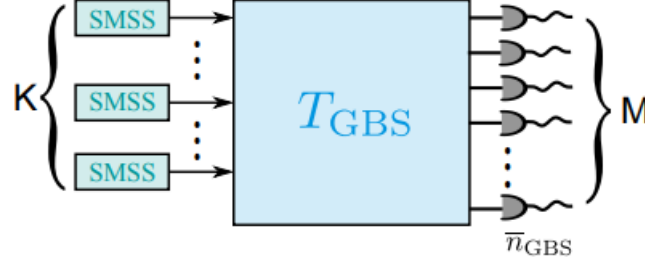


Figure 2.3: Gaussian Boson Sampler, Source:[23]

To initiate the description of the covariance matrix for  $K$  single-mode squeezed states as described in [24], a symplectic form of squeezing transformation is applied to a vacuum state which is represented by  $\frac{\mathbb{1}_{2M}}{2}$ . The squeezing matrix is defined as follows:

$$S = \begin{bmatrix} \bigoplus_{j=1}^M \cosh r_j & \bigoplus_{j=1}^M \sinh r_j \\ \bigoplus_{j=1}^M \sinh r_j & \bigoplus_{j=1}^M \cosh r_j \end{bmatrix} \quad (2.18)$$

The squeezing transformation of the initial covariance matrix yields  $\sigma = \frac{1}{2}SS^\dagger$ . Unlike the previous protocols where the unitary of an interferometer was applied directly to the state ket, in this case, we must consider the unitary transformation of the covariance matrix, as illustrated below:

$$\sigma = \frac{1}{2} \begin{bmatrix} T & 0 \\ 0 & T^* \end{bmatrix} SS^\dagger \begin{bmatrix} T^\dagger & 0 \\ 0 & T^t \end{bmatrix} \quad (2.19)$$

The transformed covariance matrix serves as our input to equation (2.14) for generating the sampling matrix  $A$ , which is then employed as an argument for the Hafnian after appropriate reduction ( $A_S$ ). The reduction of the sampling matrix is carried out based on the output photon pattern. Specifically, if there is no photon detected in the  $j^{th}$  mode, then the corresponding row and column number  $j$  and  $j+M$  are eliminated from the final covariance matrix. Moreover, the calculated sampling matrix  $A$  is found to be of the form  $A = B \oplus B^*$ .

$A$  is the direct sum of two matrices, and the hafnian of such a matrix is given by the product of hafnians of the two sub-matrices. This enables us to reformulate equation (2.16) in the following form:

$$\Pr(\bar{n}) = \frac{1}{\bar{n}! \sqrt{|\sigma|}} |\text{Haf}(B_S)|^2 \quad (2.20)$$

Here,  $B_S$  is obtained by applying a similar reduction strategy as earlier. The only difference is that we delete only the  $j^{\text{th}}$  column and row if no photon is detected in the  $j^{\text{th}}$  mode.

Up to this point, we've examined a Gaussian state with a zero displacement. However, when the displacement vector is non-zero, certain modifications are introduced to the equations, as outlined in[23]. We'll address each of these changes individually, starting with the modification reflected in the Q function of the multimode Gaussian state, which is now defined as:

$$Q_{\rho}(\alpha, \alpha^*) = \frac{1}{\sqrt{|\pi\sigma_Q|}} e^{-\frac{1}{2}(\alpha_\nu - d_\nu)^\dagger \sigma_Q^{-1} (\alpha_\nu - d_\nu)} \quad (2.21)$$

Where  $d_\nu$  is a  $2M$ -dimensional displacement vector. Following the same analysis as in the earlier case, we arrive at the following expression for the probability of obtaining  $\bar{n}$ :

$$\Pr(\bar{n}) = \frac{e^{-\frac{1}{2}d_\nu^\dagger \sigma_Q^{-1} d_\nu}}{\bar{n}! \sqrt{|\sigma_Q|}} \prod_{j=1}^M \left( \frac{\partial^2}{\partial \alpha_j \partial \alpha_j^*} \right)^{n_j} e^{\frac{1}{2} \alpha_\nu^\dagger A \alpha_\nu + F \alpha_\nu} \Bigg|_{\alpha_\nu=0} \quad \text{where } F = d_\nu^\dagger \sigma_Q^{-1} \quad (2.22)$$

It is evident that when we expand derivatives, additional terms arise due to the presence of the linear term  $F\alpha_\nu$ , in contrast to the zero displacement case. Consequently, more partitions, such as first-order terms in  $\alpha_j$  and  $\alpha_j^*$ , contribute to the final result. After detailed analysis, as elucidated in[23], the expression for calculating the probability of an output pattern  $\bar{n}$  is now given by:

$$\Pr(\bar{n}) = \frac{e^{-\frac{1}{2}d_\nu^\dagger \sigma_Q^{-1} d_\nu}}{\bar{n}! \sqrt{|\sigma_Q|}} \left\{ \text{Haf}(A_S) + \sum_{j_1, j_2, j_1 \neq j_2} F_{j_1} F_{j_2} \text{Haf}(A_{S-\{j_1, j_2\}}) + \cdots + \prod_{j=1}^{2N} F_j \right\} \quad (2.23)$$

The interpretation of this result is straightforward. The first term accounts for all the photons originating from squeezed/thermal states (covariance matrix), while the last term only encompasses contributions from the coherent state (displacement operator). The middle terms represent a mixing of photon contributions from both the squeezed/thermal and coherent components of the state. An alternative expression for the above formula can be presented in terms of what we refer to as the Loop Hafnian.

$$\Pr(\bar{n}) = \frac{e^{-\frac{1}{2}d_\nu^\dagger \sigma_Q^{-1} d_\nu}}{\bar{n}! \sqrt{|\sigma_Q|}} \text{Lhaf}(A_S, d_r) \quad (2.24)$$

Here,  $d_r$  represents the reduced displacement vector, which is obtained from  $d_\nu$  by excluding the  $j^{\text{th}}$  and  $(j + M)^{\text{th}}$  entries, as previously done for an output mode without any photons.

In terms of graph theory, the distinction between a hafnian and a loop hafnian lies in the fact that the former counts the number of perfect matchings in a loopless graph, whereas the latter has the additional capability to perform the same task on graphs with loops.

In the more general scenario where there is more than one photon in the output modes, [23] elegantly addresses the absence of a direct formula linking the hafnian to the probability. The authors propose a clever approach: distributing the surplus photons into virtual modes such that each virtual mode contains only one photon. They then apply the hafnian formula to a new matrix constructed by repeating the rows and columns of the original matrix to appropriate dimensions. It is important to note that while this new matrix does not represent a quantum covariance matrix, it effectively allows the use of the hafnian machinery to compute probabilities for a multiphoton case.

After examining the model, we must address the question of whether the Gaussian Boson Sampler (GBS) solves a computationally hard problem. The answer for the exact case of GBS is straightforward. Hafnian, being a more general matrix function than the permanent, places GBS in the  $\#P$  complexity class. This implies that if a classical algorithm existed to sample from the exact distribution of a GBS, it would imply a collapse in the polynomial hierarchy—an outcome highly implausible.

In the case of considering multiple photons in the same mode, the complexity results remain unchanged. This is because the probabilities are still dependent on the hafnian of a matrix that has been duplicated by repeating rows and columns, meaning that the rank of the matrix remains the same, and there is no change in the complexity of the problem.

The question of whether Approximate Gaussian Boson Sampling (GBS) solves a computationally hard problem is more complex and involves additional considerations. In the case of the Boson Sampling protocol, Aaronson and Arkhipov established that the Approximate Boson Sampling probability  $|GPE|_{\pm}^2$  falls within the  $BPP^{NP^O}$  complexity class. They then utilized two conjectures, assuming them to be true, which implied that  $P^{\#P} = BPP^{NP}$  unless Approximate Boson Sampling is in  $\#P$ . Similar lines of argument have been followed in [23, 17] to suggest that GBS is in  $\#P$ , but a complete proof remains an open question.

### 2.3.1 Experimental Factors - GBS

From an experimental standpoint, the GBS protocol presents several advantages over previous protocols. Firstly, the probability of generating certain photon pair events is significantly higher (exponentially) compared to protocols such as SBS and other post-selection Boson Sampling (BS) protocols. Additionally, the number of squeezers required to implement GBS is lower (quadratically) than what is required in the SBS protocol.

Another advantageous aspect of the GBS protocol is its propensity to exhibit better generation probabilities in the high photon number regime. This tendency makes it feasible to reach a regime where 50-100 photons can be generated at reasonable rates. In this regime,

the Boson Sampling problem becomes particularly interesting, as it becomes increasingly challenging to simulate it classically.

## 2.4 Non Gaussian Boson Sampling

Sampling from pure single-mode non-Gaussian states represents an extension of previous work and introduces a new theoretical framework in the field. The information presented in this section is primarily derived from [25], which introduces a new protocol for the Boson Sampling problem using the widest possible range of single-mode states. This protocol enables sampling from Non-Gaussian states, expanding the applicability to sample from states associated with higher order non quadratic Hamiltonians.

The procedure to construct an arbitrary pure single-mode photonic state is provided in [26]. This method involves the use of two squeezing operations, a set of displacement operations, and some single photon subtractions. Mathematically, the series of operations to generate the desired state can be expressed in the form given below:

$$|\psi\rangle = \hat{S}(-r) \hat{a} \hat{D}(\alpha_N) \dots \hat{a} \hat{D}(\alpha_2) \hat{a} \hat{S}(r) |0\rangle \quad (2.25)$$

Here,  $r$  is the squeezing parameter, and squeezing and anti-squeezing operations are applied at the beginning and end of the series of operations. The set of  $\alpha_i$  represents the amount of displacements needed after every step with photon subtraction. The values of  $\alpha$  are determined by an algorithm described in [26]. A pictorial representation of the scheme to generate states is provided below:

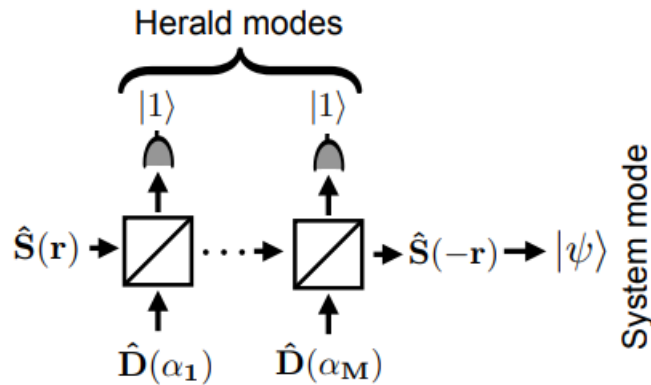


Figure 2.4: Method of constructing single mode Non-Gaussian states, Source:[25]

At each step, as the light travels through a series of highly transmitting (low reflecting) beam splitters, the state of light is combined with displaced vacuums, and a photon is detected in each of the output arms. The photon subtraction operator  $\hat{a}$  can be understood, in physical terms, as a photon detection operation, particularly in the low probability

limit. The nature of this technique is probabilistic, which means that for successful state generation, all detectors need to detect one photon each. However, this scenario is unlikely, making this technique impractical for experimental purposes. Nonetheless, it is utilized in calculating the output probability of obtaining photon patterns resulting from the interference of such states.

The Non-Gaussian Boson Sampling (NGBS) protocol integrates the Gaussian Boson Sampling (GBS) with the previously described generation technique to sample from non-Gaussian input states.

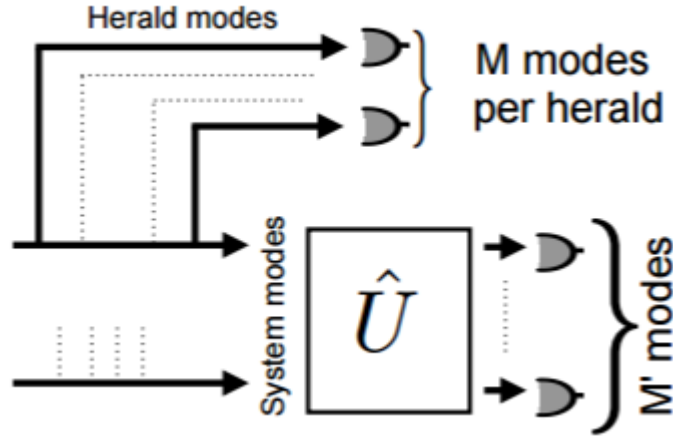


Figure 2.5: Non-Gaussian Boson Sampler, Source:[25]

A Non-Gaussian Boson Sampler, as illustrated in the figure above, consists of  $K$  non-Gaussian states, each having  $M$  modes. Out of these,  $M-1$  modes act as herald modes where photon detection takes place, and the last one is the system mode that undergoes an  $M' \times M'$  mode interferometer. Consequently, there are a total of  $M' + K(M-1)$  modes, with each of the  $K$  system modes represented by their covariance matrices ( $\sigma_{NG}$ ) and displacement vectors ( $d_{NG}$ ) before measuring the herald modes. The overall input state can be expressed in terms of this individual state information as follows:

$$\Sigma_{in} = \sigma_{NG}^{\oplus K} \oplus \mathbf{I}/2_{M'-K} \quad \text{and} \quad \Delta_{in} = d_{NG}^{\oplus K} \oplus \mathbf{0}_{M'-K} \quad (2.26)$$

The system modes enter the interferometer, and the resulting output state is represented by the following covariance matrix and displacement vector:

$$\Sigma_{out} = (U_{M'} \oplus \mathbf{I}_{(M-1)K}) \Sigma_{in} (U_{M'}^\dagger \oplus \mathbf{I}_{(M-1)K}) \quad (2.27)$$

$$\Delta_{out} = (U_{M'} \oplus \mathbf{I}_{(M-1)K}) \Delta_{in} \quad (2.28)$$

Finally, the system and herald states are measured in the photon number basis, thus giving rise to our desired Non-Gaussian Boson Sampling scheme. The NGBS scheme is directly



related to the GBS scheme in terms of measuring the photon pattern  $\bar{n}$  given that the herald modes measure 1 photon each. This conditional probability can be formulated using Bayes' theorem as follows:

$$\Pr(\bar{n}_{system} | \mathbf{1}_{herald}) = \frac{\Pr(\bar{n}_{system} \cap \mathbf{1}_{herald})}{(\Pr(\mathbf{1}_{herald}))^K} \quad (2.29)$$

In the expression above, the probability in the numerator and denominator can be calculated in the same manner as described in the Gaussian Boson Sampling (GBS) protocol.

$$\Pr(\bar{n}_{system} \cap \mathbf{1}_{herald}) = \frac{\exp(-\frac{1}{2}\Delta_{out}\Sigma_Q^{-1}\Delta_{out})}{\bar{n}_{sys}!\sqrt{|\Sigma_Q|}} \text{Lhaf}(A_s^T, F_s^T) \quad (2.30)$$

$$\Pr(\mathbf{1}_{herald}) = \frac{\exp(-\frac{1}{2}d_{NG}\sigma_{Q,NG}^{-1}d_{NG})}{\sqrt{|\sigma_Q|}} \text{Lhaf}(A_s^{NG}, F_s^{NG}) \quad (2.31)$$

The primary result of [25] lies in the calculation of the probability of a photon pattern from an array of non-Gaussian states. It is emphasized that the Non-Gaussian Boson Sampling (NGBS) problem is not asserted to have any complexity advantages. This implies that sampling from non-Gaussian states is not inherently more challenging than sampling from Gaussian states. Therefore, the earlier complexity results derived for Gaussian Boson Sampling (GBS) are applicable in the case of NGBS as well.

### 2.4.1 Experimental Factors - NGBS

All the aforementioned experimental limitations, such as the low efficiency of photon detectors, photon loss in the optical network, and the generation of input states of light as described in previous protocols, are applicable to the Non-Gaussian Boson Sampling scheme as well.

Additionally, the input state construction in this model relies on a probabilistic model [25], which further contributes to the model's limitations. While the authors demonstrate in [26] that the non-Gaussian state generation scheme approaches unity fidelity as the transmission coefficient of beam splitters approaches one, it's crucial to acknowledge the challenge of approximating an infinite-dimensional state through finite truncation in the photon number basis. Regardless of the chosen parameters, this approximation results in a created state with fidelity below unity, posing a potential source of error in the presented protocol.

---

## Our Methodology

We are presently involved in investigating the interference patterns displayed by a particular family of Non-Gaussian states. As part of this initiative, we have established a Python repository that facilitates the simulation of arbitrary instances within this family of states. This platform provides us with the capability to observe and analyze the resulting photon patterns in the output channels of an interferometer.

### 3.1 Non Gaussian States of Light

Sophisticated quantum technologies necessitate scalable and controllable quantum resources. Multimode light Gaussian states, such as squeezed states and cluster states, provide scalable quantum systems that can be generated on demand. However, Non-Gaussian features are crucial in numerous quantum protocols, especially for attaining a quantum computational advantage [27].

In the previous chapter, we explored a specific method for constructing arbitrary single-mode Non-Gaussian states through the implementation of photon subtraction techniques at beam splitters. The Non-Gaussian states of particular interest in this study are characterized by the following form:

$$|\psi\rangle = \frac{1}{\sqrt{N+1}} \sum_{n=0}^N |n\rangle \quad (3.1)$$

We confine the summation to  $N$  values of 2 or 3, which enables us to compute probabilities on a classical computer without a significant increase in the program's runtime.

### 3.2 Simulating Boson Sampling on a Classical Computer

In this section, we will present the outcomes resulting from the interference of the states mentioned earlier, within a specific interferometer which is represented mathematically by

a Fourier matrix. For convenience, we'll refer to this as the Fourier interferometer from now on. Following this, we will proceed to analytically validate these results by applying our theoretical understanding of Quantum Optics.

### 3.2.1 Two Mode Interference

As a simplified model, we will begin by examining the interference pattern resulting from two modes in a Fourier interferometer, represented by the following unitary matrix:

$$U = \frac{1}{\sqrt{2}} \begin{bmatrix} 1 & 1 \\ 1 & -1 \end{bmatrix}$$

1.  $\frac{1}{\sqrt{2}} (|0\rangle + |1\rangle)$

When two such states are subjected to a two-channel Fourier interferometer, it produces the following output pattern. Here,  $n_1$  and  $n_2$  represent the number of photons measured in the output modes 1 and 2, respectively.

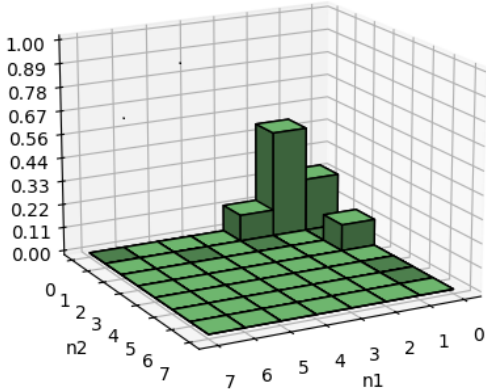


Figure 3.1: Photon Distribution

Photon Pattern	Probability
(0, 0)	0.250
(0, 2)	0.125
(1, 0)	0.500
(2, 0)	0.125

Table 3.1: Probability

2.  $\frac{1}{\sqrt{3}} (|0\rangle + |1\rangle + |2\rangle)$

By introducing an additional ket  $|2\rangle$  into the input state, we are expanding the size of the state space, and the outcomes of its probability distribution are provided below:

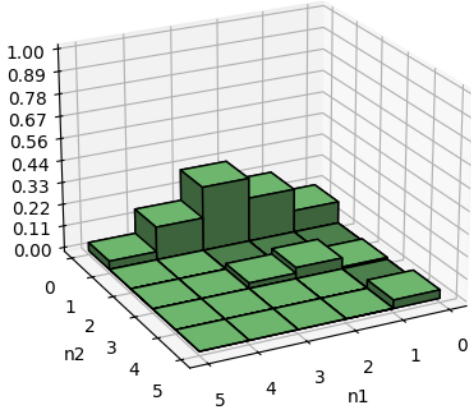


Figure 3.2: Photon Distribution

Photon Pattern	Probability
(0, 0)	0.111
(0, 2)	0.009
(0, 4)	0.041
(1, 0)	0.222
(1, 2)	0.055
(2, 0)	0.323
(2, 2)	0.027
(3, 0)	0.166
(4, 0)	0.041

Table 3.2: Probability

3.  $\frac{1}{\sqrt{4}} (|0\rangle + |1\rangle + |2\rangle + |3\rangle)$

By further increasing the size of input state space, we can still explore all possible scenarios regarding the photon's output position without sacrificing any information.

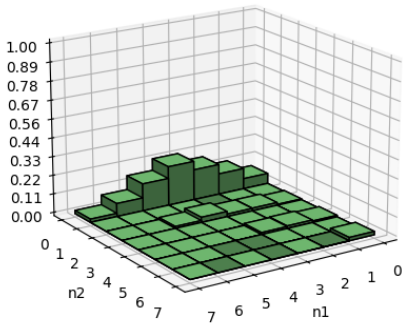


Figure 3.3: Photon Distribution

Photon Pattern	Probability
(0, 0)	0.062
(0, 2)	0.005
(0, 4)	0.009
(0, 6)	0.019
(1, 0)	0.125
(1, 2)	0.016
(1, 4)	0.015
(2, 0)	0.182
(2, 2)	0.015
(2, 4)	0.011
(3, 0)	0.233
(3, 2)	0.031
(4, 0)	0.162
(4, 2)	0.011
(5, 0)	0.078
(6, 0)	0.019

Table 3.3: Probability

### 3.2.2 Three Mode Interference

Now, let's focus on the interference pattern for three modes in a three channel Fourier interferometer, represented by the following Fourier Matrix.

$$F = \frac{1}{\sqrt{3}} \begin{bmatrix} 1 & 1 & 1 \\ 1 & \omega & \omega^2 \\ 1 & \omega^2 & \omega^4 \end{bmatrix}$$

In the Fourier Matrix, the elements 1,  $\omega$ , and  $\omega^2$  represent the complex cube roots of unity.

1.  $\frac{1}{\sqrt{2}} (|0\rangle + |1\rangle)$

When these states undergo interference in the Fourier interferometer, it generates the subsequent output pattern. In this context,  $n_1$ ,  $n_2$ , and  $n_3$  signify the counts of photons measured in the output modes 1, 2, and 3, respectively.

Photon Pattern	Probability
(0, 0, 0)	0.125
(0, 1, 1)	0.125
(1, 0, 0)	0.375
(1, 1, 1)	0.041
(2, 0, 0)	0.250
(3, 0, 0)	0.027
(0, 3, 0)	0.027
(0, 0, 3)	0.027

2.  $\frac{1}{\sqrt{3}} (|0\rangle + |1\rangle + |2\rangle)$

Now, let's introduce an additional contributing ket to the input state and pass it through the interferometer. As a consequence, it produces the subsequent output pattern.

Photon Pattern	Probability	Photon Pattern	Probability
(0, 0, 0)	0.037	(0, 0, 3)	0.010
(0, 0, 6)	0.004	(0, 1, 1)	0.006
(0, 1, 4)	0.008	(0, 2, 2)	0.037
(0, 3, 0)	0.010	(0, 3, 3)	0.0009
(0, 4, 1)	0.008	(0, 6, 0)	0.004
(1, 0, 0)	0.111	(1, 0, 3)	0.002
(1, 1, 1)	0.012	(1, 1, 4)	0.005
(1, 2, 2)	0.012	(1, 3, 0)	0.002
(1, 4, 1)	0.005	(2, 0, 0)	0.215
(2, 0, 3)	0.004	(2, 1, 1)	0.037
(2, 2, 2)	0.004	(2, 3, 0)	0.004
(3, 0, 0)	0.226	(3, 0, 3)	0.0009
(3, 1, 1)	0.032	(3, 3, 0)	0.0009
(4, 0, 0)	0.143	(4, 1, 1)	0.005
(5, 0, 0)	0.041	(6, 0, 0)	0.004

3.  $\frac{1}{\sqrt{4}} (|0\rangle + |1\rangle + |2\rangle + |3\rangle)$

This marks the point where significant computational challenges arise on a classical computer, as attempting to compute all output scenarios leads to a substantial increase in memory allocation and runtime complexity.

### 3.2.3 Four Mode Interference

We persist in our exploration, seeking to grasp the interference pattern for 4 input modes when subjected to a Fourier interferometer. The representation of this four-channelled interferometer is encapsulated by the following  $4 \times 4$  unitary matrix:

$$F = \frac{1}{\sqrt{4}} \begin{bmatrix} 1 & 1 & 1 & 1 \\ 1 & \omega & \omega^2 & \omega^3 \\ 1 & \omega^2 & \omega^4 & \omega^6 \\ 1 & \omega^4 & \omega^6 & \omega^9 \end{bmatrix}$$

1.  $\frac{1}{\sqrt{2}} (|0\rangle + |1\rangle)$

When four such states interfere within a Fourier interferometer, it produces the following output pattern. Here,  $n_1$ ,  $n_2$ ,  $n_3$ , and  $n_4$  represent the counts of photons measured in the output modes 1, 2, 3, and 4, respectively.

Photon Pattern	Probability	Photon Pattern	Probability
(0, 0, 0, 0)	0.062	(0, 0, 0, 4)	0.005
(0, 0, 1, 2)	0.031	(0, 0, 2, 0)	0.031
(0, 0, 4, 0)	0.005	(0, 1, 0, 1)	0.062
(0, 1, 2, 1)	0.007	(0, 2, 0, 2)	0.003
(0, 2, 1, 0)	0.031	(0, 4, 0, 0)	0.005
(1, 0, 0, 0)	0.249	(1, 0, 1, 2)	0.007
(1, 0, 2, 0)	0.031	(1, 1, 0, 1)	0.062
(1, 2, 1, 0)	0.007	(2, 0, 0, 0)	0.281
(2, 0, 2, 0)	0.003	(2, 1, 0, 1)	0.007
(3, 0, 0, 0)	0.093	(4, 0, 0, 0)	0.005

2.  $\frac{1}{\sqrt{3}}(|0\rangle + |1\rangle + |2\rangle)$

Incorporating an extra ket in the input state for four-mode interference is impractical, as it leads to a significant escalation in both memory allocation and runtime complexity.

These findings provide the initial indication of the distinct clustering behavior of photons, which is evident across all analyzed cases.

### 3.3 Analytical Results

We will leverage the theoretical insights gained in Quantum Optics thus far to validate a subset of the results emphasized in the preceding section.

#### 3.3.1 Two Mode Calculation

Let's pick a simple example of two state kets  $\frac{1}{\sqrt{2}}(|0\rangle + |1\rangle)$  interfering in a Fourier interferometer, represented by the following unitary matrix:

$$U = \frac{1}{\sqrt{2}} \begin{bmatrix} 1 & 1 \\ 1 & -1 \end{bmatrix}$$

This unitary matrix establishes a relationship between the operators of the output and input modes.

$$\begin{bmatrix} \hat{c} \\ \hat{d} \end{bmatrix} = \frac{1}{\sqrt{2}} \begin{bmatrix} 1 & 1 \\ 1 & -1 \end{bmatrix} \begin{bmatrix} \hat{a} \\ \hat{b} \end{bmatrix}$$

In this context,  $\hat{c}$  and  $\hat{d}$  denote the photon annihilation operators of the output modes. It's important to recall that annihilation operators subtract one photon from a Fock state,

while creation operators  $\hat{c}^\dagger$  and  $\hat{d}^\dagger$  add one photon to it. Utilizing this understanding, we can formulate our input state in terms of operators and vacuum state, as presented below:

$$|\psi\rangle_{in} = \frac{1}{2} (\mathbf{1}_a + \hat{a}^\dagger) (\mathbf{1}_b + \hat{b}^\dagger) |0, 0\rangle_{a,b}$$

Now, let's apply the transformation relations for the mode operators in the output channels.

$$\hat{a} = \frac{1}{\sqrt{2}} (\hat{c} + \hat{d})$$

$$\hat{b} = \frac{1}{\sqrt{2}} (\hat{c} - \hat{d})$$

This enables us to express the state of light in the output channel as follows:

$$|\psi\rangle_{out} = \frac{1}{2} \left( \mathbf{1}_c + \frac{\hat{c}^\dagger}{\sqrt{2}} + \frac{\hat{d}^\dagger}{\sqrt{2}} \right) \left( \mathbf{1}_d + \frac{\hat{c}^\dagger}{\sqrt{2}} - \frac{\hat{d}^\dagger}{\sqrt{2}} \right) |0, 0\rangle_{c,d}$$

Upon straightforward simplification of this expression, we arrive at the ultimate form of the output state ket, as follows:

$$|\psi\rangle_{out} = \frac{1}{2} |0, 0\rangle + \frac{1}{\sqrt{2}} |1, 0\rangle + \frac{1}{2\sqrt{2}} |2, 0\rangle - \frac{1}{2\sqrt{2}} |0, 2\rangle$$

By applying the postulates of Quantum Mechanics, we can compute the probability of measuring  $(n_1, n_2)$  photons in the output channels, as described in the equation below.

$$P(n_1, n_2) = |\langle n_1, n_2 | \psi \rangle_{out}|^2 \quad (3.2)$$

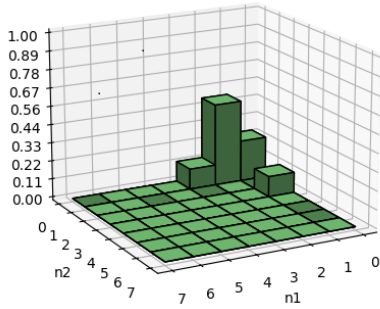


Figure 3.4: Photon Distribution

Photon Pattern	Amplitude	Probability
(0, 0)	$\frac{1}{2}$	0.25
(1, 0)	$\frac{1}{\sqrt{2}}$	0.5
(2, 0)	$\frac{1}{2\sqrt{2}}$	0.125
(0, 2)	$\frac{1}{2\sqrt{2}}$	0.125

Table 3.4: Probability

### 3.3.2 Three Mode Calculation

To simplify, we will once more select the state  $\frac{1}{\sqrt{2}} (|0\rangle + |1\rangle)$ . However, this time, three instances of this state will undergo interference in a Fourier interferometer, represented by the following matrix:



$$F = \frac{1}{\sqrt{3}} \begin{bmatrix} 1 & 1 & 1 \\ 1 & \omega & \omega^2 \\ 1 & \omega^2 & \omega^4 \end{bmatrix}$$

The annihilation operators for the three output channels are denoted as  $\hat{e}$ ,  $\hat{f}$ , and  $\hat{g}$ , and their respective transformation relation with the input mode operators is presented below:

$$\begin{bmatrix} \hat{e} \\ \hat{f} \\ \hat{g} \end{bmatrix} = \frac{1}{\sqrt{3}} \begin{bmatrix} 1 & 1 & 1 \\ 1 & \omega & \omega^2 \\ 1 & \omega^2 & \omega^4 \end{bmatrix} \begin{bmatrix} \hat{a} \\ \hat{b} \\ \hat{c} \end{bmatrix}$$

Using the properties of annihilation and creation operators we can write the construct the input state as prescribed below:

$$|\psi\rangle_{in} = \frac{1}{2\sqrt{2}} (\mathbf{1}_a + \hat{a}^\dagger) (\mathbf{1}_b + \hat{b}^\dagger) (\mathbf{1}_c + \hat{c}^\dagger) |0, 0, 0\rangle_{a,b,c}$$

To express the output state, we need to invert the relation (3.15) and represent the input mode operators in terms of the output ones. Upon inversion and Hermitian conjugation, we obtain the following relations:

$$\begin{aligned} \hat{a}^\dagger &= \frac{1}{\sqrt{3}} (\hat{e}^\dagger + \hat{f}^\dagger + \hat{g}^\dagger) \\ \hat{b}^\dagger &= \frac{1}{\sqrt{3}} (\hat{e}^\dagger + \omega \hat{f}^\dagger + \omega^2 \hat{g}^\dagger) \\ \hat{c}^\dagger &= \frac{1}{\sqrt{3}} (\hat{e}^\dagger + \omega^2 \hat{f}^\dagger + \omega \hat{g}^\dagger) \end{aligned}$$

Utilizing the aforementioned relations, we can express the output state as follows:

$$\begin{aligned} |\psi\rangle_{out} &= \frac{1}{2\sqrt{2}} \left( \mathbf{1}_e + \frac{1}{\sqrt{3}} (\hat{e}^\dagger + \hat{f}^\dagger + \hat{g}^\dagger) \right) \left( \mathbf{1}_e + \frac{1}{\sqrt{3}} (\hat{e}^\dagger + \omega \hat{f}^\dagger + \omega^2 \hat{g}^\dagger) \right) \\ &\quad \left( \mathbf{1}_e + \frac{1}{\sqrt{3}} (\hat{e}^\dagger + \omega^2 \hat{f}^\dagger + \omega \hat{g}^\dagger) \right) |0, 0, 0\rangle_{e,f,g} \end{aligned}$$

It is evident that this seemingly straightforward problem, when approached analytically, becomes intricate. The expansion involves 64 terms, encompassing 30 distinct kets that form the output state. Nevertheless, it is fascinating to note that only 8 of these unique ket combinations possess non-zero probabilities. We will forego the details of this extensive calculation and present the final output state, as described below:

$$\begin{aligned}
|\psi\rangle_{out} = & \frac{1}{2\sqrt{2}} |0, 0, 0\rangle - \frac{1}{2\sqrt{2}} |0, 1, 1\rangle + \sqrt{\frac{3}{8}} |1, 0, 0\rangle - \frac{1}{\sqrt{24}} |1, 1, 1\rangle \\
& + \frac{1}{2} |2, 0, 0\rangle + \frac{1}{6} |3, 0, 0\rangle + \frac{1}{6} |0, 3, 0\rangle + \frac{1}{6} |0, 0, 3\rangle
\end{aligned}$$

The probability of the wavefunction collapsing into one of the constituent  $|n_1, n_2, n_3\rangle$  kets is also the probability of measuring  $n_1$ ,  $n_2$ , and  $n_3$  number of photons in the output channels, respectively.

$$P(n_1, n_2, n_3) = |\langle n_1, n_2, n_3 | \psi \rangle_{out}|^2 \quad (3.3)$$

We can observe that the theoretical calculations precisely align with our experimental data, as demonstrated in the table below. The significant observation of photon bunching indicates a strong indication of an underlying quantum effect within this experiment.

Photon Pattern	Amplitude	Probability
(0, 0, 0)	$\frac{1}{2\sqrt{2}}$	0.125
(0, 1, 1)	$-\frac{1}{2\sqrt{2}}$	0.125
(1, 0, 0)	$\sqrt{\frac{3}{8}}$	0.375
(1, 1, 1)	$-\frac{1}{\sqrt{24}}$	0.041
(2, 0, 0)	$\frac{1}{2}$	0.250
(3, 0, 0)	$\frac{1}{6}$	0.027
(0, 3, 0)	$\frac{1}{6}$	0.027
(0, 0, 3)	$\frac{1}{6}$	0.027

### 3.3.3 Four Mode Calculation

We can replicate the same method, which is straightforward but extensive, as employed in previous sections to generate results for the interference pattern of 4 modes using any arbitrary unitary matrix. However, conducting these calculations manually become highly cumbersome due to the exponential growth in the number of terms during the expansion of the output state ket.

In a manner analogous to the three-mode scenario, where we had 64 terms ( $4^3$ ) in the expansion of the output state, we would encounter 625 terms ( $5^4$ ) in the expansion of the output state for a four-mode scenario, assuming the unitary matrix is an arbitrary matrix with most of its elements nonzero. In practical terms, manually expressing the output state in a four-mode interference instance becomes nearly impossible.

In this chapter, we demonstrated the practical implementation of **Non-Gaussian Boson Sampling**, showcasing the execution of Boson Sampling on Non-Gaussian states. We also

delved into the theoretical and experimental challenges of the Boson Sampling problem, emphasizing the capabilities of optical quantum architectures and manifesting the concept of **Quantum Supremacy**.

---

## Observation of Photon Bunching

In the previous chapter, we gained insight into the operational dynamics of Boson Sampling on non-Gaussian states, shedding light on its computational inefficiency when implemented on classical computers. We also observed a crucial phenomenon: significant photon bunching occurred for higher numbers of modes and larger input states.

In this chapter, we aim to shed further light on this underlying effect and analyze its consequences in a more structured manner. Before moving forward, it's essential to recall the Hong-Ou-Mandel Effect, which posits that when two photons are passed, one in each arm of a balanced beam splitter, both photons arrive in a bunch at either of the output arms. In an ideal scenario, the probability of simultaneously detecting photons in both output arms diminishes to zero. We are trying to investigate a similar phenomenon in a broader context, involving multimode input states and any arbitrary interferometer configuration.

However, for the sake of simplification and to provide a tangible illustration of the effect, we will consider a scenario where a specific input state,  $\frac{1}{\sqrt{2}}(|0\rangle + |1\rangle)$ , is passed into each of the  $N$  input arms, and the interferometer is represented by an  $N$ -mode Fourier matrix. Extending this analysis to any other state and interferometer configuration is then straightforward.

We will repeat the same procedure as in the previous chapter and aim to discern trends in the data by introducing a ratio of the number of output states possessing non-zero probability of detection to the total number of states that could be generated in this particular setting.

$$|\psi\rangle_{in} = \frac{1}{\sqrt{2^N}} (\mathbf{1}_{a_1} + \hat{a}_1^\dagger) (\mathbf{1}_{a_2} + \hat{a}_2^\dagger) \cdots (\mathbf{1}_{a_N} + \hat{a}_N^\dagger) |0, 0, \dots, 0\rangle_{a_1, a_2, \dots, a_N} \quad (4.1)$$

The unitary transformation between operators of the input and output modes is given by the following matrix equation:

---


$$\begin{bmatrix} \hat{b}_1 \\ \hat{b}_2 \\ \hat{b}_3 \\ \hat{b}_4 \\ \vdots \\ \hat{b}_N \end{bmatrix} = \frac{1}{\sqrt{N}} \begin{bmatrix} 1 & 1 & 1 & \cdots & 1 \\ 1 & \omega & \omega^2 & \cdots & \omega^{N-1} \\ 1 & \omega^2 & \omega^4 & \cdots & \omega^{2N-2} \\ 1 & \omega^3 & \omega^6 & \cdots & \omega^{3N-3} \\ \vdots & \vdots & \vdots & \ddots & \vdots \\ 1 & \omega^{N-1} & \omega^{2N-2} & \cdots & \omega^{N^2-2N+1} \end{bmatrix} \begin{bmatrix} \hat{a}_1 \\ \hat{a}_2 \\ \hat{a}_3 \\ \hat{a}_4 \\ \vdots \\ \hat{a}_N \end{bmatrix} \quad (4.2)$$

The output state after passing through this interferometer can be formulated as follows (Note:  $\hat{U}$  in the equation below represents the unitary matrix representing the interferometer, and  $\hat{a}$  and  $\hat{b}$  are the column vectors of the mode operators).

$$|\psi\rangle_{out} = \frac{1}{\sqrt{2^N}} \left( \mathbf{1}_{b_1} + [\hat{U}^{-1}\hat{b}]_1^\dagger \right) \left( \mathbf{1}_{b_2} + [\hat{U}^{-1}\hat{b}]_2^\dagger \right) \cdots \left( \mathbf{1}_{b_N} + [\hat{U}^{-1}\hat{b}]_N^\dagger \right) |0, 0, \dots, 0\rangle_{b_1, b_2, \dots, b_N} \quad (4.3)$$

With this general formula, we can calculate the number of distinct state kets that we can theoretically obtain in the output channels, or in other words, we can determine the total number of output photon patterns. Let's denote this number by  $\bar{N}$ , and considering the constraint that we can't detect more than  $N$  photons combined in all the output detectors, calculating  $\bar{N}$  simplifies to a straightforward solution of the permutation formula given below:

$$\bar{N} = \left| \left\{ (n_1, n_2, n_3, \dots, n_N) \mid 0 \leq n_1 + n_2 + n_3 + \dots + n_N \leq N \right\} \right| \quad (4.4)$$

Where  $n_1, n_2, \dots, n_N$  represent the number of photons detected in the respective output channels.

However, according to our observations, we understand that not all combinations of output photon patterns carry non-zero probabilities. A significant portion of these combinations experience destructive interference, resulting in their cancellation. As a result, only a few combinations retain non-zero probabilities, leading to the observation of significant photon bunching. Let's represent the number of unique combinations that actually persist after transformation through the interferometer as  $\bar{n}$ .

We determine the value of  $\bar{n}$  from the simulations we conducted earlier, and we utilize this value in computing our desired ratio of interest,  $R$ .

$$R = \frac{\bar{n}}{\bar{N}} \quad (4.5)$$

With this understanding, we will apply this theory to calculate the aforementioned ratio for several toy multimode instances and attempt to identify any trends in the data. In addition to computing the ratio ( $R$ ), we are also interested in calculating the correlation matrix for each instance. This matrix encodes the correlation value between each pair of output modes. The correlation value between modes  $i$  and  $j$  is determined by the following equation:

$$c_{i,j} = \langle n_i n_j \rangle - \langle n_i \rangle \langle n_j \rangle \quad (4.6)$$

$$c_{i,j} = \sum_{n_i, n_j} P(n_i, n_j) n_i n_j - \sum_{n_i} P(n_i) n_i \sum_{n_j} P(n_j) n_j \quad (4.7)$$

Hence, the correlation matrix is a collection of such values and takes the following form:

$$C = \begin{bmatrix} c_{0,0} & c_{0,1} & c_{0,2} & \cdots & c_{0,N-1} \\ c_{1,0} & c_{1,1} & c_{1,2} & \cdots & c_{1,N-1} \\ c_{2,0} & c_{2,1} & c_{2,2} & \cdots & c_{2,N-1} \\ \vdots & \vdots & \vdots & \ddots & \vdots \\ c_{N-1,0} & c_{N-1,1} & c_{N-1,3} & \cdots & c_{N-1,N-1} \end{bmatrix} \quad (4.8)$$

#### 4.0.1 Two Modes

For two modes,  $\bar{N}$  is straightforward and is given by the following equation:

$$\bar{N} = \left| \left\{ (n_1, n_2) \mid 0 \leq n_1 + n_2 \leq 2 \right\} \right|$$

$$\bar{N} = 6$$

whereas,  $\bar{n} = 4$  as determined from the results computed in the previous chapter.

$R = 0.67$	Photon Pattern Probability	
$C = \begin{bmatrix} 0.4375 & -0.1875 \\ -0.1875 & 0.4375 \end{bmatrix}$	(0, 0)	0.250
	(0, 2)	0.125
	(1, 0)	0.500
	(2, 0)	0.125

Table 4.1: Probability

## 4.0.2 Three Modes

$$\bar{N} = \left| \left\{ (n_1, n_2, n_3) \mid 0 \leq n_1 + n_2 + n_3 \leq 3 \right\} \right|$$

$$\bar{N} = 20$$

whereas,  $\bar{n} = 8$  as determined from the results computed in the previous chapter.

			<b>Photon Pattern</b>	<b>Probability</b>
$R = 0.40$			(0, 0, 0)	0.125
			(0, 1, 1)	0.125
			(1, 0, 0)	0.375
			(1, 1, 1)	0.041
			(2, 0, 0)	0.250
			(3, 0, 0)	0.027
			(0, 3, 0)	0.027
			(0, 0, 3)	0.027

$$C = \begin{bmatrix} 0.666 & -0.208 & -0.208 \\ -0.208 & 0.354 & 0.104 \\ -0.208 & 0.104 & 0.354 \end{bmatrix}$$

Table 4.2: Probability

## 4.0.3 Four Modes

$$\bar{N} = \left| \left\{ (n_1, n_2, n_3, n_4) \mid 0 \leq n_1 + n_2 + n_3 + n_4 \leq 4 \right\} \right|$$

$$\bar{N} = 70$$

whereas,  $\bar{n} = 20$  as determined from the results computed in the previous chapter.

<b>Photon Pattern</b>	<b>Probability</b>	<b>Photon Pattern</b>	<b>Probability</b>
(0, 0, 0, 0)	0.062	(0, 0, 0, 4)	0.005
(0, 0, 1, 2)	0.031	(0, 0, 2, 0)	0.031
(0, 0, 4, 0)	0.005	(0, 1, 0, 1)	0.062
(0, 1, 2, 1)	0.007	(0, 2, 0, 2)	0.003
(0, 2, 1, 0)	0.031	(0, 4, 0, 0)	0.005
(1, 0, 0, 0)	0.249	(1, 0, 1, 2)	0.007
(1, 0, 2, 0)	0.031	(1, 1, 0, 1)	0.062
(1, 2, 1, 0)	0.007	(2, 0, 0, 0)	0.281
(2, 0, 2, 0)	0.003	(2, 1, 0, 1)	0.007
(3, 0, 0, 0)	0.093	(4, 0, 0, 0)	0.005

---


$$C = \begin{bmatrix} 0.906 & -0.218 & -0.218 & -0.218 \\ -0.218 & 0.343 & 0.031 & 0.093 \\ -0.218 & 0.031 & 0.406 & 0.031 \\ -0.218 & 0.093 & 0.031 & 0.343 \end{bmatrix} \quad \boxed{R = 0.28}$$

#### 4.0.4 Five Modes

$$\bar{N} = \left\{ (n_1, n_2, n_3, n_4, n_5) \mid 0 \leq n_1 + n_2 + n_3 + n_4 + n_5 \leq 5 \right\}$$

$$\bar{N} = 252$$

Although we didn't present the results for the case of 5 modes in the previous chapter, here is the data obtained from the simulation of 5 modes, which gives us  $\bar{n} = 52$ .

Photon Pattern	Probability	Photon Pattern	Probability
(0, 0, 0, 0, 0)	0.031	(0, 0, 0, 0, 5)	0.001
(0, 0, 0, 1, 3)	0.007	(0, 0, 0, 2, 1)	0.012
(0, 0, 0, 5, 0)	0.001	(0, 0, 1, 0, 2)	0.012
(0, 0, 1, 1, 0)	0.031	(0, 0, 1, 3, 1)	0.001
(0, 0, 2, 1, 2)	0.0009	(0, 0, 2, 2, 0)	0.005
(0, 0, 3, 0, 1)	0.007	(0, 0, 5, 0, 0)	0.001
(0, 1, 0, 0, 1)	0.031	(0, 1, 0, 2, 2)	0.0009
(0, 1, 0, 3, 0)	0.007	(0, 1, 1, 0, 3)	0.001
(0, 1, 1, 1, 1)	0.001	(0, 1, 2, 0, 0)	0.012
(0, 1, 3, 1, 0)	0.001	(0, 2, 0, 0, 2)	0.005
(0, 2, 0, 1, 0)	0.012	(0, 2, 1, 2, 0)	0.0009
(0, 2, 2, 0, 1)	0.0009	(0, 3, 0, 1, 1)	0.001
(0, 3, 1, 0, 0)	0.007	(0, 5, 0, 0, 0)	0.001
(1, 0, 0, 0, 0)	0.156	(1, 0, 0, 1, 3)	0.001
(1, 0, 0, 2, 1)	0.009	(1, 0, 1, 0, 2)	0.009
(1, 0, 1, 1, 0)	0.056	(1, 0, 2, 2, 0)	0.001
(1, 0, 3, 0, 1)	0.001	(0, 0, 0, 0, 5)	0.056
(1, 1, 0, 3, 0)	0.001	(1, 1, 1, 1, 1)	0.0002
(1, 1, 2, 0, 0)	0.009	(1, 2, 0, 0, 2)	0.001
(1, 2, 0, 1, 0)	0.009	(1, 3, 1, 0, 0)	0.001
(2, 0, 0, 0, 0)	0.250	(2, 0, 0, 2, 1)	0.001
(2, 0, 1, 0, 2)	0.001	(2, 0, 1, 1, 0)	0.022
(2, 1, 0, 0, 1)	0.022	(2, 1, 2, 0, 0)	0.001
(2, 2, 0, 1, 0)	0.001	(3, 0, 0, 0, 0)	0.150
(3, 0, 1, 1, 0)	0.001	(3, 1, 0, 0, 1)	0.001
(4, 0, 0, 0, 0)	0.030	(5, 0, 0, 0, 0)	0.001



---


$$C = \begin{bmatrix} 1.149 & -0.225 & -0.225 & -0.225 & -0.225 \\ -0.225 & 0.337 & 0.024 & 0.024 & 0.087 \\ -0.225 & 0.024 & 0.337 & 0.087 & 0.024 \\ -0.225 & 0.024 & 0.087 & 0.337 & 0.024 \\ -0.225 & 0.087 & 0.024 & 0.024 & 0.337 \end{bmatrix} \quad \boxed{R = 0.206}$$

#### 4.0.5 Six Modes

$$\bar{N} = \left\{ (n_1, n_2, n_3, n_4, n_5, n_6) \mid 0 \leq n_1 + n_2 + n_3 + n_4 + n_5 + n_6 \leq 6 \right\}$$

$$\bar{N} = 924$$

Due to practical constraints, we won't present the extensive data for six modes here. Nonetheless, the essential parameter is computed from the program as  $\bar{n} = 130$ .

$$C = \begin{bmatrix} 1.325 & -0.214 & -0.215 & -0.214 & -0.215 & -0.214 \\ -0.214 & 0.324 & 0.021 & 0.021 & 0.002 & 0.083 \\ -0.215 & 0.021 & 0.324 & 0.021 & 0.083 & 0.021 \\ -0.214 & 0.021 & 0.021 & 0.387 & 0.021 & 0.021 \\ -0.215 & 0.021 & 0.083 & 0.021 & 0.324 & 0.021 \\ -0.214 & 0.083 & 0.021 & 0.021 & 0.021 & 0.324 \end{bmatrix} \quad \boxed{R = 0.140}$$

Computations for more than six modes could not be executed on a classical computer, underscoring the complexity of this problem even for such a seemingly simple input configuration.

#### 4.0.6 Diminishing Trend

While the computational challenges are significant, our main focus lies in understanding the trend of decreasing  $R$  as we increase the number of input modes. This trend provides valuable insights into the behavior of the system.

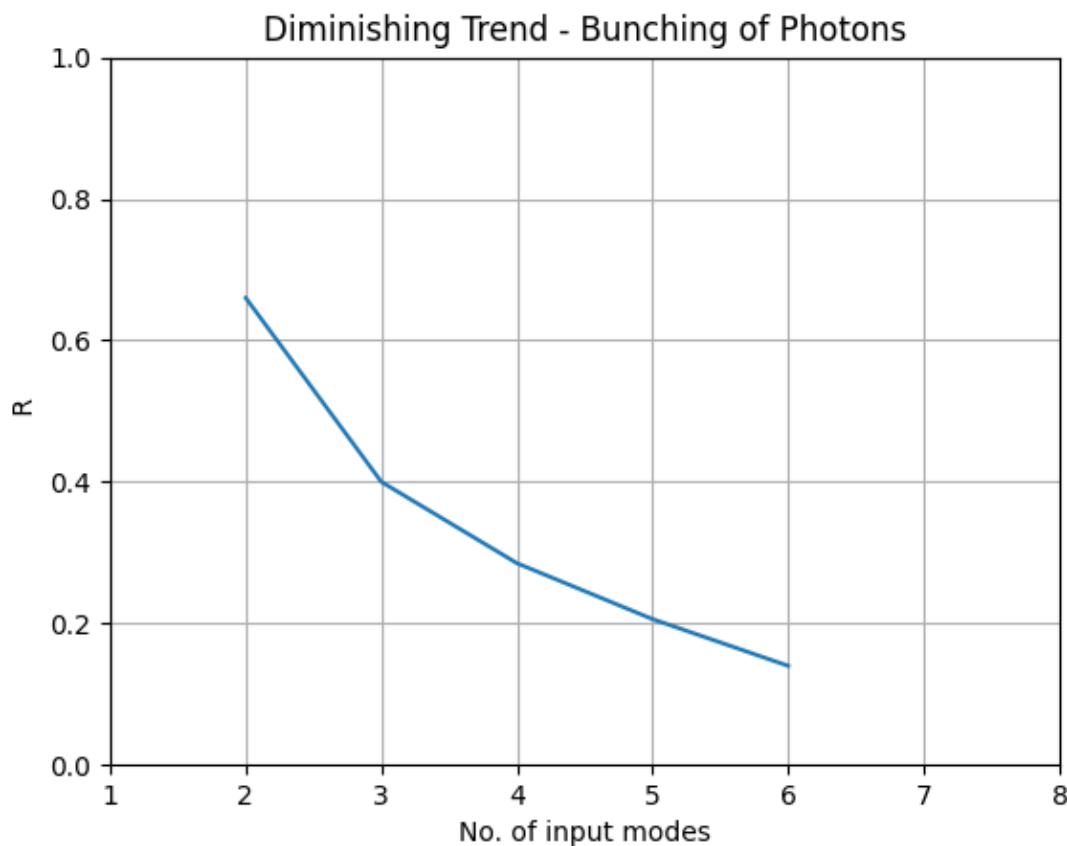


Figure 4.1: Decreasing Trend

While further data collection exceeds our current computational capabilities, the observed trend strongly indicates that as the number of modes increases, the ratio  $R$  will approach a value very close to zero. This analysis aligns with the findings established in [28], [29], and [30], which describe the suppression laws for multiparticle interference in various classes of interferometers.

#### 4.0.7 Correlation Analysis using Random Interferometers

We further endeavor to deepen our understanding of non-Gaussian Boson Sampling by conducting a series of simulations. In these simulations, we utilize arbitrary interferometers (random unitaries) instead of confining ourselves to Fourier interferometers. The setup involves configuring the first two input modes as  $\frac{1}{\sqrt{2}} (|0\rangle + |1\rangle)$ , while the remaining input modes are initialized with vacuum states  $|0\rangle$ .

Let's denote the number of vacuum modes in each instance by  $M$  and plot a histogram of the correlation value  $C_{12}$  for the first two output modes, according to equation (4.7), for 1000 different random unitaries.

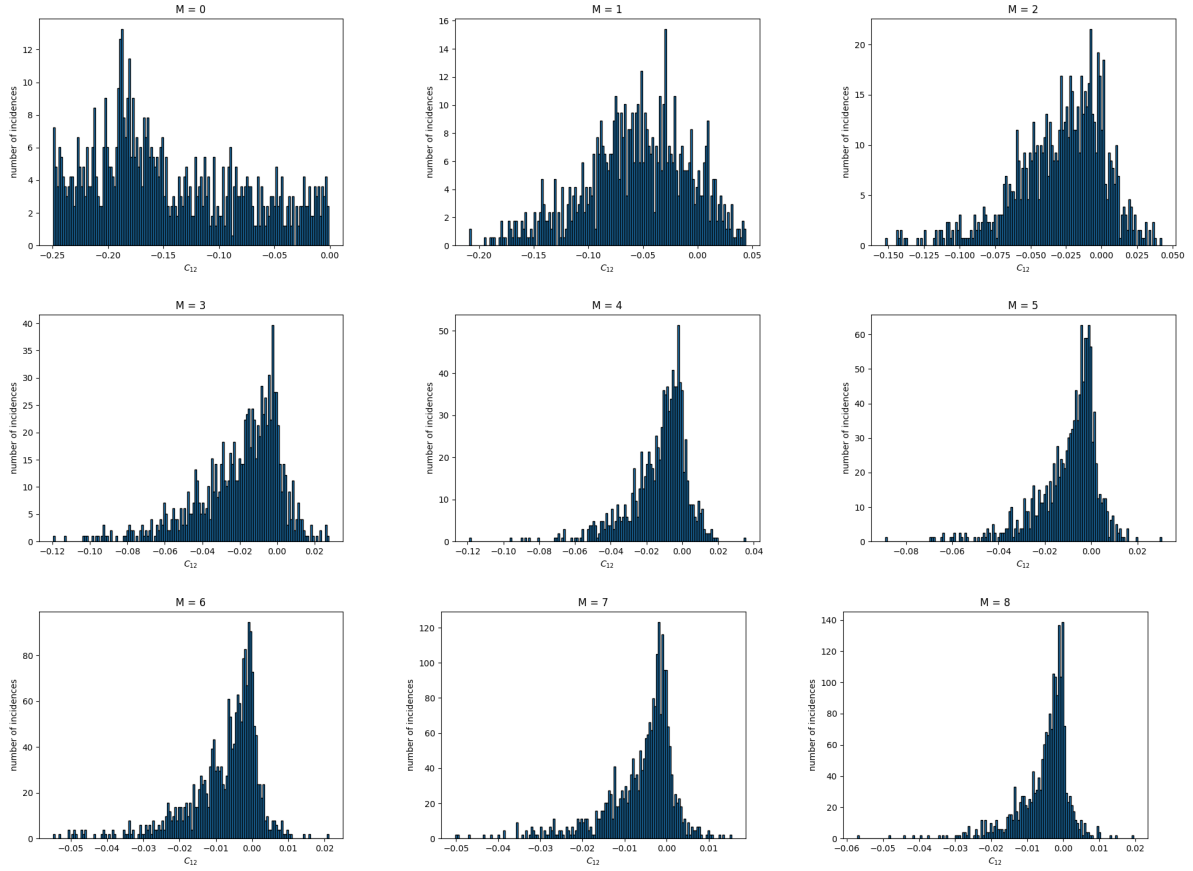


Figure 4.2: Histogram of correlation values  $C_{12}$  for different numbers of vacuum states,  $M$  ranging from 0 to 8.

As we increase  $M$ , we observe the histogram of correlation values  $C_{12}$  developing a peak structure. This peak sharpens with higher values of  $M$ , and its center shifts towards zero. This trend suggests that increasing the number of vacuum modes in the input results in a decrease in the correlation between the first two output modes. Our analysis expands upon the benchmarking techniques outlined in [31], encompassing a wider range of quantum states as well as classical states. In addition, we also explore the negative correlation values, contrasting with [31], where the analysis is exclusively focused on positive correlation values.

---

## Conclusions

In summary, our journey commenced with an exploration of the quantum description of light, revisiting the theoretical foundations of Quantum Optics. We then delved into the construction of models for the Boson Sampling Problem, tracing its evolution over time. Finally, we reached our focal point of interest: **Non-Gaussian Boson Sampling**.

The primary objective of this thesis was to comprehend the interference behavior of a particular family of non-Gaussian states of light when subjected to an interferometer. The major results of this work can be broadly categorized into two types.

1. **Quantum Supremacy:** The simulations and data presented in Chapter 3 offer compelling evidence that Boson Sampling from non-Gaussian states poses a computationally challenging problem. Classical computers demonstrate inefficiency in handling large configurations. Consequently, a Boson Sampler, although a non-universal model of a quantum processor, tends to exhibit Quantum Supremacy.
2. **Bunching of Photons:** In Chapter 4, it becomes evident that there exists a generalized quantum phenomenon akin to the Hong-Ou-Mandel effect for non-Gaussian states of light interfering within an interferometer. We observed significant bunching of photons in almost all instances of computation. The majority of photons undergo destructive interference, resulting in very few output combinations retaining a non-zero probability of detection. As the number of input states increases, we also observed a sharp decline in the ratio of non-zero probability output states to the total possible output states. This ratio tends to a value very close to zero as  $n \rightarrow \infty$ .

---

## Future Direction of Work

At this stage, we could elevate the performance of our project by addressing various crucial aspects. This strategic focus is pivotal in ensuring not only improved results but also positioning ourselves favorably for the publication of noteworthy findings.

1. A crucial aspect that demands attention is the computational efficiency of the project. Although the current program provides accurate results, its computational scalability is constrained, preventing us from computing probabilities for instances with more than six modes due to resource limitations on our standard classical computer. To effectively address this limitation, it is crucial to explore optimal algorithms that can leverage the low rank of the Non-Gaussian Boson Sampling problem. Our current algorithm, which revolves around the concept of Loop Hafnians, relies on substantial data structures for problem-solving.
2. Another major focus of the project centers on exploring the applications of Boson Sampling. While we are accumulating compelling evidence that the Boson Sampler exhibits inherent computational speedup or Quantum Supremacy, the practical implications of this speedup remain uncertain. This open question is a highly active area of research in numerous laboratories worldwide. Our intention is to delve into this area once our primary goals are achieved.

---

## Bibliography

- [1] Loudon, R. *The Quantum Theory of Light*. Oxford: Clarendon Press, second edition, 1983.
- [2] Planck, M. On an Improvement of Wien's Equation for the Spectrum, *Verh. dtsch. phys. Ges. Berlin* 2,202-4. 1900.
- [3] Planck, M. On the Theory of the Energy Distribution Law of the Normal Spectrum *ibid* , 237-45. 1900.
- [4] Einstein, A. On a Heuristic Viewpoint Concerning the Production and Transformation of Light. *Annalen der Physik*, 17, 132-148. 1905.
- [5] Straumann, N. Einstein in 1916: "On the Quantum Theory of Radiation". 2017, 1703.08176.
- [6] Dirac, P. The Quantum Theory of the Emission and Absorption of Radiation. *Proc. Roy. Soc.*, A114,243. 1927.
- [7] Maiman, T. H. Stimulated Optical Radiation in Ruby. *Nature* 187, 493–494 (1960). Available from: <https://doi.org/10.1038/187493a0>
- [8] Glauber, R. J. The Quantum Theory of Optical Coherence. *Phys. Rev.*, volume 130, Jun 1963: pp. 2529–2539, doi:10.1103/PhysRev.130.2529. Available from: <https://link.aps.org/doi/10.1103/PhysRev.130.2529>
- [9] Nielsen, M. A.; Chuang, I. L. *Quantum Computation and Quantum Information: 10th Anniversary Edition*. Cambridge University Press, 2010.
- [10] Aaronson, S.; Arkhipov, A. The Computational Complexity of Linear Optics. 2010, 1011.3245.
- [11] Lund, A. P.; Laing, A.; Rahimi-Keshari, S.; et al. Boson Sampling from a Gaussian State. *Phys. Rev. Lett.*, volume 113, Sep 2014: p. 100502, doi:10.1103/

- PhysRevLett.113.100502. Available from: <https://link.aps.org/doi/10.1103/PhysRevLett.113.100502>
- [12] Reck, M.; Zeilinger, A.; Bernstein, H. J.; et al. Experimental realization of any discrete unitary operator. *Phys. Rev. Lett.*, volume 73, Jul 1994: pp. 58–61, doi: 10.1103/PhysRevLett.73.58. Available from: <https://link.aps.org/doi/10.1103/PhysRevLett.73.58>
- [13] Lounis, B.; Orrit, M. Single-photon sources. *Reports on Progress in Physics*, volume 68, no. 5, May 2005: pp. 1129–1179, doi:10.1088/0034-4885/68/5/R04.
- [14] Rohde, P. P.; Ralph, T. C. Error tolerance of the boson-sampling model for linear optics quantum computing. *Phys. Rev. A*, volume 85, Feb 2012: p. 022332, doi: 10.1103/PhysRevA.85.022332. Available from: <https://link.aps.org/doi/10.1103/PhysRevA.85.022332>
- [15] Menicucci, N. C.; Ma, X.; Ralph, T. C. Arbitrarily Large Continuous-Variable Cluster States from a Single Quantum Nondemolition Gate. *Phys. Rev. Lett.*, volume 104, Jun 2010: p. 250503, doi:10.1103/PhysRevLett.104.250503. Available from: <https://link.aps.org/doi/10.1103/PhysRevLett.104.250503>
- [16] Silverstone, J. W.; Bonneau, D.; Ohira, K.; et al. On-chip quantum interference between silicon photon-pair sources. *Nature Photonics*, volume 8, no. 2, dec 2013: pp. 104–108, doi:10.1038/nphoton.2013.339.
- [17] Hamilton, C. S.; Kruse, R.; Sansoni, L.; et al. Gaussian Boson Sampling. *Physical Review Letters*, volume 119, no. 17, oct 2017, doi:10.1103/physrevlett.119.170501.
- [18] Ferraro, A.; Olivares, S.; Paris, M. G. A. Gaussian states in continuous variable quantum information. 2005, [quant-ph/0503237](https://arxiv.org/abs/quant-ph/0503237).
- [19] Barnett, S. M.; Radmore, P. *Methods in Theoretical Quantum Optics*. Oxford University Press, 1996.
- [20] Schleich, W. P. *Quantum Optics in Phase Space*. John Wiley & Sons, 2011.
- [21] Caianiello, E. R. *Combinatorics and renormalization in quantum field theory*, volume 38. Reading: Benjamin, 1973, ISBN 978-0-8053-1646-9, 978-0-8053-1645-2.
- [22] Caianiello, E. R. *Il Nuovo Cimento 10*, volume 1. 1953.
- [23] Kruse, R.; Hamilton, C. S.; Sansoni, L.; et al. Detailed study of Gaussian boson sampling. *Physical Review A*, volume 100, no. 3, sep 2019, doi:10.1103/physreva.100.032326.

- 
- [24] Simon, R.; Mukunda, N.; Dutta, B. Quantum-noise matrix for multimode systems:  $U(n)$  invariance, squeezing, and normal forms. *Phys. Rev. A*, volume 49, Mar 1994: pp. 1567–1583, doi:10.1103/PhysRevA.49.1567. Available from: <https://link.aps.org/doi/10.1103/PhysRevA.49.1567>
- [25] Hamilton, C. S.; Jex, I. Boson Sampling from Non-Gaussian States. 2024, 2403.17183.
- [26] Fiurášek, J.; García-Patrón, R.; Cerf, N. J. Conditional generation of arbitrary single-mode quantum states of light by repeated photon subtractions. *Phys. Rev. A*, volume 72, Sep 2005: p. 033822, doi:10.1103/PhysRevA.72.033822. Available from: <https://link.aps.org/doi/10.1103/PhysRevA.72.033822>
- [27] Ra, Y.-S.; Dufour, A.; Walschaers, M.; et al. Non-Gaussian quantum states of a multimode light field. *Nature Physics*, volume 16, no. 2, Dec. 2019: p. 144–147, ISSN 1745-2481, doi:10.1038/s41567-019-0726-y. Available from: <http://dx.doi.org/10.1038/s41567-019-0726-y>
- [28] Crespi, A. Suppression laws for multiparticle interference in Sylvester interferometers. *Phys. Rev. A*, volume 91, Jan 2015: p. 013811, doi:10.1103/PhysRevA.91.013811. Available from: <https://link.aps.org/doi/10.1103/PhysRevA.91.013811>
- [29] Tichy, M. C.; Tiersch, M.; de Melo, F.; et al. Zero-transmission law for multiport beam splitters. *Physical Review Letters*, volume 104, no. 22, 2010: p. 220405.
- [30] Viggianiello, N.; Flamini, F.; Innocenti, L.; et al. Experimental generalized quantum suppression law in Sylvester interferometers. *New Journal of Physics*, volume 20, no. 3, mar 2018: p. 033017, doi:10.1088/1367-2630/aaad92. Available from: <https://dx.doi.org/10.1088/1367-2630/aaad92>
- [31] Phillips, D. S.; Walschaers, M.; Renema, J. J.; et al. Benchmarking of Gaussian boson sampling using two-point correlators. *Phys. Rev. A*, volume 99, Feb 2019: p. 023836, doi:10.1103/PhysRevA.99.023836. Available from: <https://link.aps.org/doi/10.1103/PhysRevA.99.023836>